eRD14 - EIC PID Consortium

- An integrated program for particle identification (PID) for a future Electron-Ion Collider (EIC) detector.

M. Alfred[10], B. Azmoun[3], F. Barbosa[15], M. Boer[4], W. Brooks[20], T. Cao[24], M. Chiu[3], E. Cisbani[13,14], M. Contalbrigo[12], S. Danagoulian[17], A. Datta[23], A. Deldotto[13], M. Demarteau[2], A. Denisov[11], J.M. Durham[16], A. Durum[11], R. Dzhygadlo[9], D. Fields[23], Y. Furletova[15], C. Gleason[24], M. Grosse-Perdekamp[22], J. Harris[25], M. Hattawy[18], X. He[8], H. van Hecke[16], T. Horn[4], J. Huang[3], C. Hyde[18], Y. Ilieva[24], G. Kalicy[4], A. Kebede[17], B. Kim[5], E. Kistenev[3], M. Liu[16], R. Majka[25], J. McKisson[15], R. Mendez[20], I. Mostafanezhad[21], P. Nadel-Turonski[19], K. Peters[9], W. Roh[8], R. Pisani[3], P. Rossi[15], M. Sarsour[8], C. Schwarz[9], J. Schwiening[9], C.L. da Silva[16], N. Smirnov[25], J. Stevens[6], A. Sukhanov[3], X. Sun[8], S. Syed[8], R. Towell[1], G. Varner[21], R. Wagner[2], C. Woody[3], C.-P. Wong[8], J. Xie[2], Z.W. Zhao[7], B. Zihlmann[15], C. Zorn[15].
Contacts: P. Nadel-Turonski <turonski@jlab.org>, Y. Ilieva <jordanka@physics.sc.edu>

[1] Abilene Christian University, Abilene, TX 79601
[2] Argonne National Lab, Argonne, IL 60439
[3] Brookhaven National Lab, Upton, NY 11973
[4] Catholic University of America, Washington, DC 20064
[5] City College of New York, New York, NY 10031
[6] College of William & Mary, Williamsburg, VA 2318
[7] Duke University, Durham, NC 27708
[8] Georgia State University, Atlanta, GA 30303
[9] GSI Helmholtzzentrum für Schwerionenforschung GmbH, 64291 Darmstadt, Germany
[10] Howard University, Washington, DC 20059
[11] Institute for High Energy Physics, Protvino, Russia
[12] INFN, Sezione di Ferrara, 44100 Ferrara, Italy
[13] INFN, Sezione di Roma, 00185 Rome, Italy
[14] Istituto Superiore di Sanità, 00161 Rome, Italy
[15] Jefferson Lab, Newport News, VA 23606
[16] Los Alamos National Lab, Los Alamos, NM 87545
[17] North Carolina A&T State University, Greensboro, NC 27411
[18] Old Dominion University, Norfolk, VA 23529
[19] Stony Brook University, Stony Brook, NY 11794
[20] Universidad Técnica Federico Santa María, Valparaíso, Chile
[21] University of Hawaii, Honolulu, HI 96822
[22] University of Illinois, Urbana-Champaign, IL 61801
[23] University of New Mexico, Albuquerque, NM 87131
[24] University of South Carolina, Columbia, SC 29208
[25] Yale University, New Haven, CT 06520

Table of Contents

1. Introduction **3**

2. Hadron identification **4**

2.1 PID requirements and implementation options 4

2.1.1 Hadron ID requirements 4

2.1.2 Integrated PID solution for the EIC (concept) detector(s) 6

2.2 Dual-radiator RICH (dRICH) 9

2.2.1 Design and simulation update 10

2.2.2 FY18 Progresses and Achievements 16

2.2.3 Proposed dRICH R&D Activities 17

2.2.4 dRICH R&D Deliverables 17

2.3 Modular Aerogel RICH (mRICH) 18

2.3.1 FY18 Progress and Achievements 18

2.3.2 Proposed mRICH R&D Activities 21

2.3.3 mRICH R&D Deliverables 21

2.4 DIRC 22

2.4.1 Summary 22

2.4.2 FY18 Progress and Achievements 23

2.4.3 Proposed DIRC R&D Activities 27

2.4.4 DIRC R&D Deliverables 29

2.5 High-resolution Time-of-Flight (TOF) 30

2.5.1 FY18 Progress and Achievements 32

3. Lepton (electron and muon) Identification **33**

4. Photosensors & Electronics **35**

4.1 Sensors in High-B fields 36

4.1.1 FY18 Progress and Achievements 36

4.1.2 Proposed High-B R&D Activities 39

4.1.3 High-B R&D Deliverables 41

4.2 LAPPD™ MCP-PMTs 41

4.2.1 FY18 Progress and Achievements 41

4.2.2 Proposed LAPPD R&D Activities 45

4.2.3 LAPPD R&D Deliverables 45

4.3 Readout Sensors and Electronics for Detector Prototypes 51

4.3.1 FY18 Progress and Achievements 47

4.3.2 Proposed R&D Deliverables 52

4.2.3 Electronics R&D Deliverables 52

5. Budget **52**

Abstract
The EIC PID consortium (eRD14) has been formed to develop an integrated program for particle identification (PID) for a future Electron-Ion Collider (EIC) detector, for which excellent particle identification is an essential requirement. For instance, identification of the hadrons in the final state is needed for understanding how different quark flavors contribute to the properties of hadrons, and reliable identification of the scattered electron is important for covering kinematics where pion backgrounds are large. The PID systems also have the greatest overall impact on the layout of the central detector and put important constraints on the magnetic field. It is thus essential to conduct the relevant R&D at an early stage of the development of a complete EIC detector. In addition to providing solutions addressing the broader EIC requirements, the PID consortium has worked closely with BNL and JLab to ensure that the R&D projects are compatible with the specific EIC detector concepts that are being pursued there.

1. Introduction

The ability to identify hadrons in the final state is a key requirement for the physics program of the EIC. Being able to tag the flavor of the struck quark in semi-inclusive DIS can, for instance, tell us something about the transverse momentum distributions (and potentially orbital angular momentum) of the strange sea, while open charm (with subsequent decays into kaons) is important for probing the distribution of gluons in protons and nuclei. While the distribution of produced particles depends on the specific process, broadly speaking the kinematics for meson production follows the energies of the colliding beams. If the reaction produces a meson traveling in the direction of the proton (ion) beam, this meson can have a momentum which is a significant fraction of that of the beam. If the meson is produced in the opposite (electron) direction, it cannot acquire more momentum than that carried by the electron beam. In the central region it is possible to produce mesons over a wide range of momenta, but the distribution is driven by the kinematics of the process (Q^2, p_T) rather than the energies of the colliding beams[1]. Here, a greater reach of the PID coverage directly translates into, for instance, a larger lever arm in Q^2 – a key goal for the EIC – as well as an ability to probe deeper into the high-p_T region of semi-inclusive DIS. In both cases (high Q^2 and high p_T) the event rates are low, but the physics impact is high. The Q^2 coverage of the detector at central angles (mid rapidity) does, however, grow quickly with the momentum of the detected (and identified) particles. To fully satisfy the physics goals of the EIC, it is thus essential to provide coverage above 5 GeV/c for hadrons (π/K) in the barrel region, with 6 – 7 GeV/c being ideal. In the electron endcap, one would need to provide hadron ID up to a significant fraction of the electron beam energy (~10 GeV/c), while in the hadron endcap one would need to reach a significant fraction of the proton or ion beam momentum (~50 GeV/c).

To address the different requirement associated with the three different parts of the detector, the consortium is pursuing R&D on (and requesting funding for) three different technologies for imaging Cherenkov detectors: a dual-radiator (gas/aerogel) RICH (dRICH) for the hadron endcap, a

[1] Note that p_T is defined with respect to the virtual photon direction in the rest frame of the proton (ion) rather than the beam direction in the detector frame. A large p_T will, generally, give rise to a higher momentum, as well as a larger component transverse to the beam, but the boost smears the distribution.

high-performance DIRC for the central (barrel) region, and a modular aerogel RICH (mRICH) for the electron endcap, which could also be used in the hadron endcap in conjunction with a single-radiator gas RICH such as the one developed by eRD6. A time-of-flight (TOF) measurement, or dE/dx information from a TPC, is also needed for PID in the momentum range below the thresholds of the Cherenkov detectors, for which the consortium has performed R&D on mRPC and MCP-PMT-based TOF systems.
The Cherenkov systems also have a significant potential for *e/π* identification. When combined with an EM calorimeter, the mRICH and DIRC could provide excellent suppression of the low-momentum charged-pion backgrounds, which limit the ability to measure the scattered electron in kinematics where it loses most of its energy (in the detector frame). The progress of the R&D for these systems is very promising, and may in the future eliminate the needs for other supplementary *e/π* identification systems (for instance, the hadronic calorimeter on the electron endcap proposed for the BeAST or an *e/π* Cherenkov/HBD proposed for the JLab detector). Being able to eliminate such potentially redundant systems would make the EIC detector simpler, more compact, and cheaper. Further improving the *e/π* capabilities of the Cherenkov detectors may thus be a natural extension of the current R&D effort (for the mRICH it could mean slightly increasing the focal length and reducing pixel size, while for the DIRC it could imply improving the time resolution and ensuring that the radiator bar length is kept as short as possible). On the hadron side, the dRICH provides a significant *e/π* identification capability (~15 GeV on its own, and more than 20 GeV when combined with the EM calorimeter), which is sufficient for the detection of, for instance, decays of charmonium states. An important recent result is that the performance does not suffer greatly even as the size of the detector is reduced. This was seen when the dRICH design was adapted to the slightly smaller space available in the BNL detectors concepts.
The PID consortium is also carrying out R&D on photosensors for the Cherenkov detectors. The challenges addressed by the PID consortium are: operations inside the magnetic field of the central detector; and cost reduction. The former is carried out using the high-B test facility at JLab, while the latter focuses on adaptation and optimization of LAPPD™ MCP-PMT's to EIC requirements (pixelated readout, UV photocathodes, high-B capabilities), as well as characterization of early-production sensors.
In FY18 we also started a new effort within the consortium to develop cutting-edge readout electronics for all the small-pixel photosensors (including the LAPPDs) that will be used by the Cherenkov detectors. This work is being led by U. Hawaii and INFN, with support from JLab. The initial version of this electronics is already being used in the 2018 mRICH beam test at Fermilab. Later versions, based on the new SiREAD chip, will form a common readout for all Cherenkov prototypes, as well as the basis for the readout of the final Cherenkov systems to be used the future EIC detector.

2. Hadron identification

2.1 PID requirements and implementation options

2.1.1 Hadron ID requirements

The physics program of the EIC, as described in the White Paper, the 2010 INT report, the 2015 NSAC Long Range Plan, and elsewhere, is very broad and multifaceted – and so are the corresponding detector requirements. The most basic particle distribution is that from inclusive Deep Inelastic Scattering (DIS),

which essentially sums over all combinations of final-state hadrons for a given kinematics (x, Q^2) of the scattered electron. As one looks at specific subsets of the data, the particle distributions can be quite different. For example, the analysis of events at the exclusive limit leads to transverse spatial imaging of the quarks and gluons in the target nucleon or ion beam, for which flavor sensitivity is crucial to unravel the chiral-symmetry-breaking structure of the sea. Here, the struck quark hadronizes into a pion or a kaon, taking essentially all of the momentum transferred from the scattered electron. In this subprocess, the kaon momenta are much higher than the average momenta for kaon production in DIS. Similarly, the intermediate case of semi-inclusive DIS allows the creation of transverse images in momentum space. Here it is also important to cover a wide range in meson momentum fraction (*vis a vis* the 'jet'), with PID for flavor separation. Failing to do so will restrict the kinematical reach of the EIC regardless of the beam energies provided by the accelerator.

Another important case to consider is when the kaons are not produced in the primary process, but are decay products of heavier mesons. For instance, the kaons from the decay of the φ-meson, which is important for studies of gluon saturation, have higher momenta than kaons from the decay of D-mesons (open charm), which also provide information on gluon distributions.

A compilation of a catalogue of processes and kinematics illustrating the impact of various kaon identification options on the full EIC physics program goes beyond the scope of this R&D proposal. A lot of information can be found in the EIC White Paper, to which we refer. However, we note that for the purpose of understanding the general hadron ID requirements at EIC, this level of detail is not necessary. As long as one keeps in mind that a lot of the information lies in the tails of the distributions, where the number of particles is small, the meson distributions from inclusive DIS provide a good guidance. Figure 2.1.1 shows these distributions for pions and kaons in a common BNL/JLab kinematics (10 GeV/c electrons on 100 GeV/c protons), in a broad but typical bin of Q^2.

As discussed in the introduction, with higher beam energies, the meson energies in the endcaps become correspondingly higher, while the distribution in the central barrel, is less affected. Figure 2.1.1 clearly shows the need for PID over a very wide momentum range (up to about 50 GeV/c) in the hadron endcap, and a moderate range up to 5–7 GeV/c in the central barrel. In the electron endcap, which also sees hadrons with higher momenta produced at lower values of Q^2, the desired range would reach somewhat higher limit than the one suggested by the Q^2-bin in Fig. 2.1.1, approaching the electron beam energy. Thus, an upper limit of about 10 GeV/c is a relatively site-independent requirement. In addition, we note that the π/K ratios are not excessive – and become smaller for higher momenta, making identification easier. Thus, when discussing the momentum reach, the relevant level of separation is 3–4 σ.

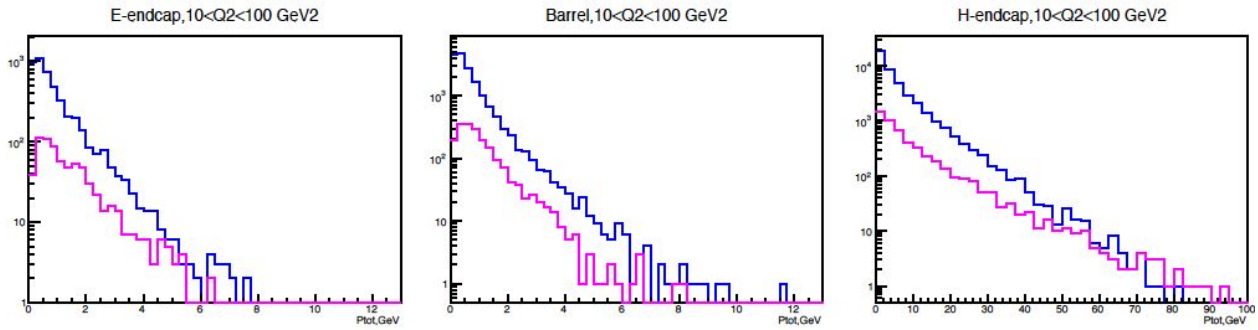


Figure 2.1.1: Momentum distributions of pions (blue) and kaons (magenta) from Pythia for DIS events corresponding to collisions between 10 GeV/*c* electrons and 100 GeV/*c* protons, a common BNL/JLab kinematics, shown for a bin of $10<Q^2<100$ GeV^2 (without imposing cuts related to any specific physics channel or analysis).

2.1.2 Integrated PID solution for the EIC (concept) detector(s)

The three model detectors developed at BNL and JLab originally had slightly different layouts of the hadron ID systems, but the configurations have converged. In particular, the layout of the BeAST detector changed in 2016, making it compatible with all the PID systems being developed by eRD14, and implementation of all three Cherenkov systems (dRICH, mRICH, and DIRC) is currently underway. The configuration of the EIC detector concept based on sPHENIX was also updated very recently. It now includes the mRICH in both the electron and hadron endcaps as well as the DIRC in the barrel. The psTOF is also an option for, in particular, the small angles on the hadron side. The inner Hcal, which is a particular feature of sPHENIX, makes it easier to use a gas-only RICH such as the one developed by eRD6, but a dual-radiator RICH (dRICH) could be used if the collision collision point was shifted, creating more space on the hadron endcap. The JLab detector concept incorporated all eRD14 technologies already from the start of the PID consortium activities. Thus, the consortium strategy of developing an integrated PID solution suited for the EIC physics requirements has not only resulted in significant progress on the hardware R&D, but also contributed to the evolution of the various EIC detector concepts proposed at BNL and JLab (shown in Figures 2.1.2–2.1.4).

Central Barrel

In addition to meeting the performance requirements, the PID system for the central has to cover a large area but with a minimal radial footprint. A DIRC detector offers an attractive solution as it can meet all three requirements. It is the most radially compact PID detector (the radiator bar thickness is less than 2 cm), and the bars can cover a large area while the sensor area remains small. Such a reduction in area can be accomplished in a conventional RICH detector by using mirrors, but this solution is not compatible with the requirement on compactness. Using recent estimates for the cost per unit area, polished fused silica is cheaper than low-cost photosensors, making DIRC overall more suitable for the barrel than, say, the mRICH. The ongoing R&D has also shown that performance can be pushed well beyond the 4 GeV/*c* achieved in BaBar, up to 5–6 GeV/*c* using advanced optics (eRD4) and to 6–7 GeV/*c* by optimizing the system for time-based reconstruction (eRD14), making the DIRC a very good match for the EIC requirements. The DIRC has thus now been adopted as a baseline solution for by the three detector concepts developed at BNL and JLab, although a high-resolution TOF could also be considered for the PID in the barrel as it is relatively compact and affordable.

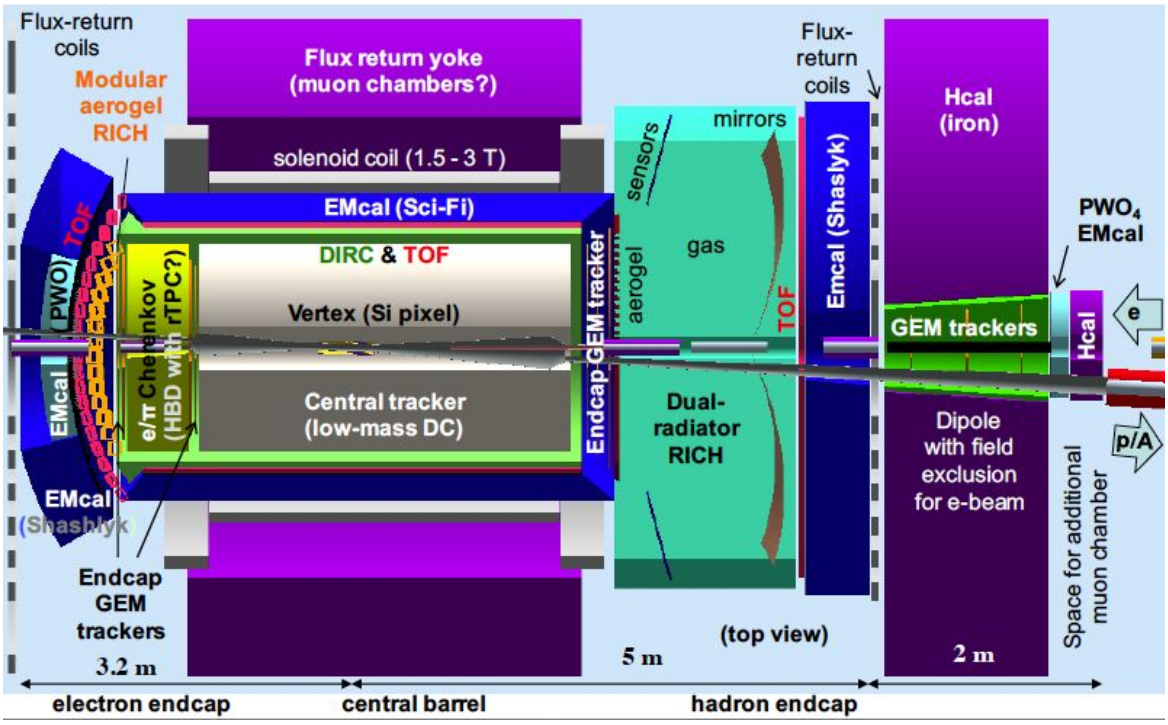


Figure 2.1.2: The JLab central detector concept uses the DIRC, dual-radiator, and modular aerogel RICH detectors from the eRD14 R&D, and has 4π TOF coverage. It also includes an *e/π* Cherenkov detector in the electron endcap for suppression of low-momentum charged pions, although the supplementary *e/π* capability of the latest version of the mRICH may turn out to be sufficient for this task.

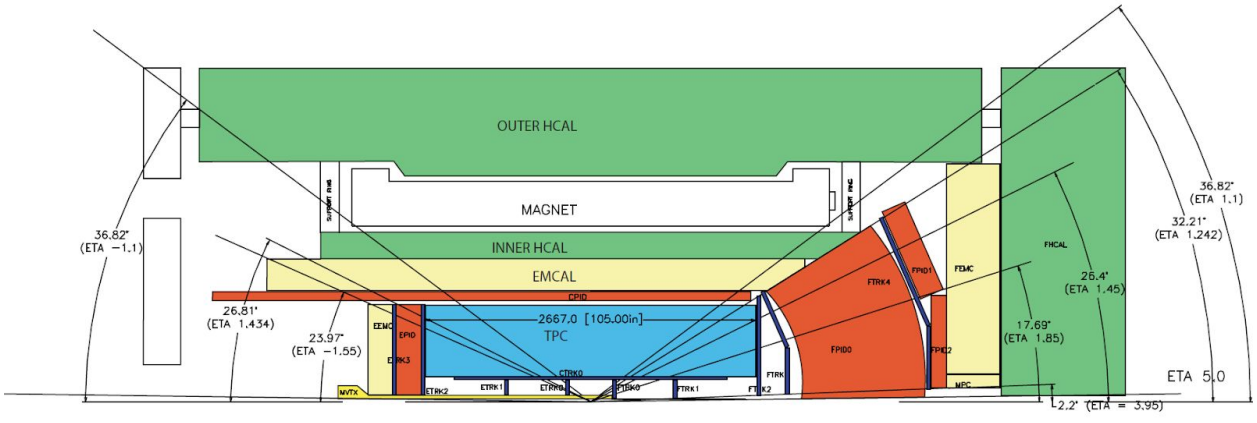


Figure 2.1.3: The 2018 version of the BNL EIC detector based on sPHENIX (which uses the BaBar solenoid) includes a DIRC at mid-rapidity and the mRICH in the electron endcap. In the hadron endcap, the current concept uses the single-radiator gas RICH developed by eRD6 in combination with the mRICH, but is also compatible with a dual-radiator RICH, such as the one developed by eRD14.

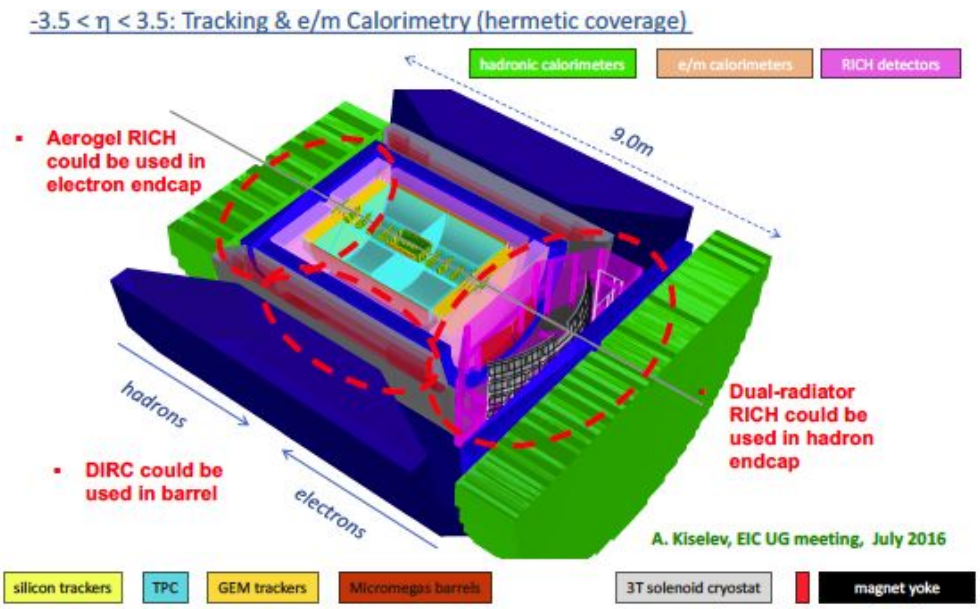


Figure 2.1.4: The BNL BeAST detector concept reserves space for several types of PID systems. Currently, all three eRD14 Cherenkov systems (DIRC, mRICH, and dRICH) are being implemented (although the figure above shows the CMB RICH from GSI which came with the simulation package).

(Outgoing) electron-side endcap

The EIC is designed to support a wide range of electron beam energies (currently assumed to be 3–12 GeV in the first stage of the JLab design and up to 18 GeV at BNL). However, hadron ID for momenta up to about 10 GeV/*c* would satisfy both the BNL and JLab requirements, making a compact, high-performance aerogel RICH a natural choice. Over the last year, such a system has become part of the baseline for all three major EIC detector concepts (JLab, ePHENIX, BeAST). In terms of implementation, there are three options. A mirror-based design, a proximity-focused design using two aerogel indices, and a lens-based aerogel RICH. However, the mirror-based option is not compact, and the proximity-focused alternative is only compact if the momentum coverage is modest. The lens-focused mRICH design, on the other hand, offers both a compact design and the desired momentum range. The lens-focusing also reduces the sensor area required per unit of solid angle, which is important since photosensors are the main cost driver of the RICH detectors.

(Outgoing) hadron-side endcap

Due to the large span of hadron momenta, ranging from a few GeV to a large fraction of the beam energy, the PID requirements on the hadron endcap are in many way the most demanding. The difference in the maximum proton-beam energies considered at the two sites is also significant (250 GeV for BNL and 100 GeV for JLab). However, even for lower beam energies the maximum hadron momenta are so large that it is important to provide good π/K separation up to several tens of GeVs. Thus, any future EIC detector will need to incorporate a mirror-based, focusing gas RICH as part of the hadron-side PID solution. From a technological point of view, the R&D path that needs to be pursued for the hadron ID is thus relatively site-independent, and a nominal 3σ π/K coverage up to 50 GeV/*c* is reasonable for both sites.

The key challenge is instead how to best cover the full momentum range. The most straightforward solution is to have a dual-radiator (gas and aerogel) RICH covering the high and mid momentum range, with supplementary coverage by TOF (or dE/dx) for the lower momenta. However, no such RICH has yet been built for a collider experiment with the strong limitations due to space and magnetic field expected for an EIC detector, making the ongoing R&D undertaken by eRD14 imperative. By combining n=1.02 aerogel and C_2F_6 gas, the dual-radiator RICH (dRICH) design pursued by eRD14 provides continuous coverage in RICH mode over the full momentum range (see Fig 2.1.5), and the layout with sector-based, outward-reflecting mirrors makes it possible to move the photosensors away from the beam.
However, the natural geometry for a dRICH is almost cylindrical, and if the layout of the other subsystems favor a more conical shape, the CF_4 gas-only RICH with inward-reflecting mirrors developed by eRD6 could be favorable. The gas-only RICH could be supplemented by separate detectors such as the mRICH (used in the current version of ePHENIX) or TOF to cover the lower momenta. The lack of continuous PID coverage in this configuration suggests, however, that further R&D may be needed, perhaps considering the use of a heavier gas with a slightly higher index of refraction.

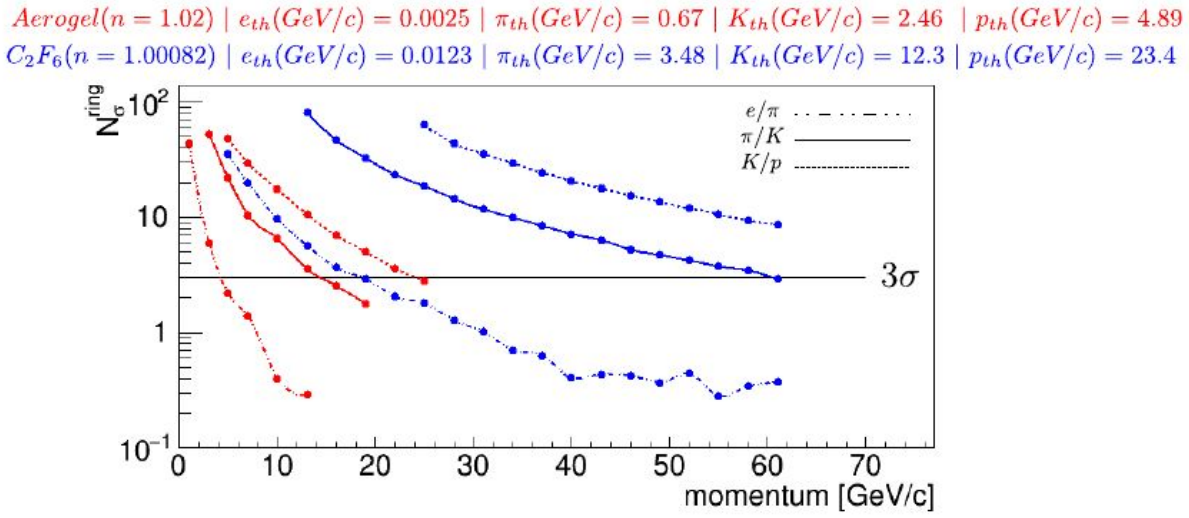


Figure 2.1.5: C_2F_6 gas/aerogel dual-radiator RICH performance for a particle scattered at 15 degrees. There is a good overlap between the PID coverage of the aerogel (red) and the gas (blue) for all three pairs of particle species.

2.2 Dual-radiator RICH (dRICH)

Contacts: Z.W. Zhao <zwzhao@jlab.org>, E. Cisbani <evaristo.cisbani@iss.infn.it>

The dual-radiator Ring Imaging Cherenkov (dRICH) detector has been designed to provide continuous full hadron identification ($\pi/K/p$, better than 3 sigma apart) from ~3 GeV/c to ~60 GeV/c and, electron identification (e/π) up to about 15 GeV/c, on the (outgoing) ion-side endcap of the EIC detector, covering angles up to 25°. Achieving this momentum coverage on the ion-side is a key requirement for the EIC physics program. The dRICH has the unique ability to provide continuous PID coverage (in RICH mode) over this full momentum range.

After the evaluation of various alternative designs, we have defined a baseline configuration for this detector to consists of two radiators (aerogel and gas) that share the same outward focusing mirror and of highly segmented (~3mm^2 pixel size) photosensors. Such a configuration with outward reflecting mirror (as compared to inward reflecting mirrors) keeps the focal plane away from the beam and ensures that the UV photons radiated in the gas go directly to the photosensors. In order to reduce the effect of aberrations caused by the spherical mirror, the photosensor surface has been optimized and designed to be a curved surface as shown in Fig. 2.2.1.

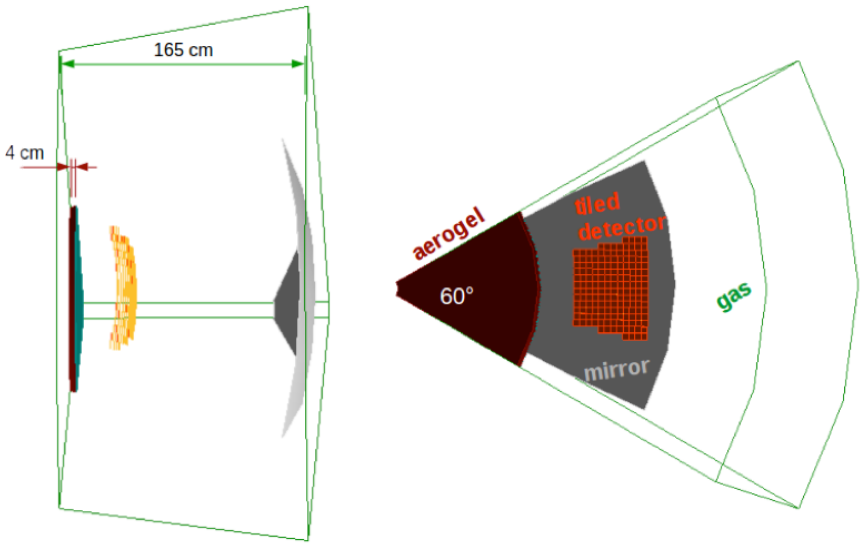


Figure 2.2.1: A single dRICH sector with slightly curved optical sensor detector surface. **Left:** side view of aerogel (dark red), mirror (light grey) and sensors (yellow); indicated are the aerogel thickness and the gas gap. **Right:** front view of aerogel (dark red), mirror (light grey) and sensors (light red).

2.2.1 Design and simulation update

The baseline design performance has been investigated and optimized with a realistic Geant4/GEMC model and related simulation, tuned with the up-to-date data from literature or recent measurements. Simulations have been analyzed by ad-hoc tools, including a track-based algorithm, which was extended more recently to an event-based Cherenkov-angle reconstruction to properly handle events with multiplicity larger than 1. Figure 2.2.2 shows the PID performances obtained by the latter method, in a semi-inclusive DIS (SIDIS) physics experimental conditions. The results of this detailed analysis confirm the design goals (see Fig. 2.2.3), however some of the adopted/proposed solutions do require further experimental studies.

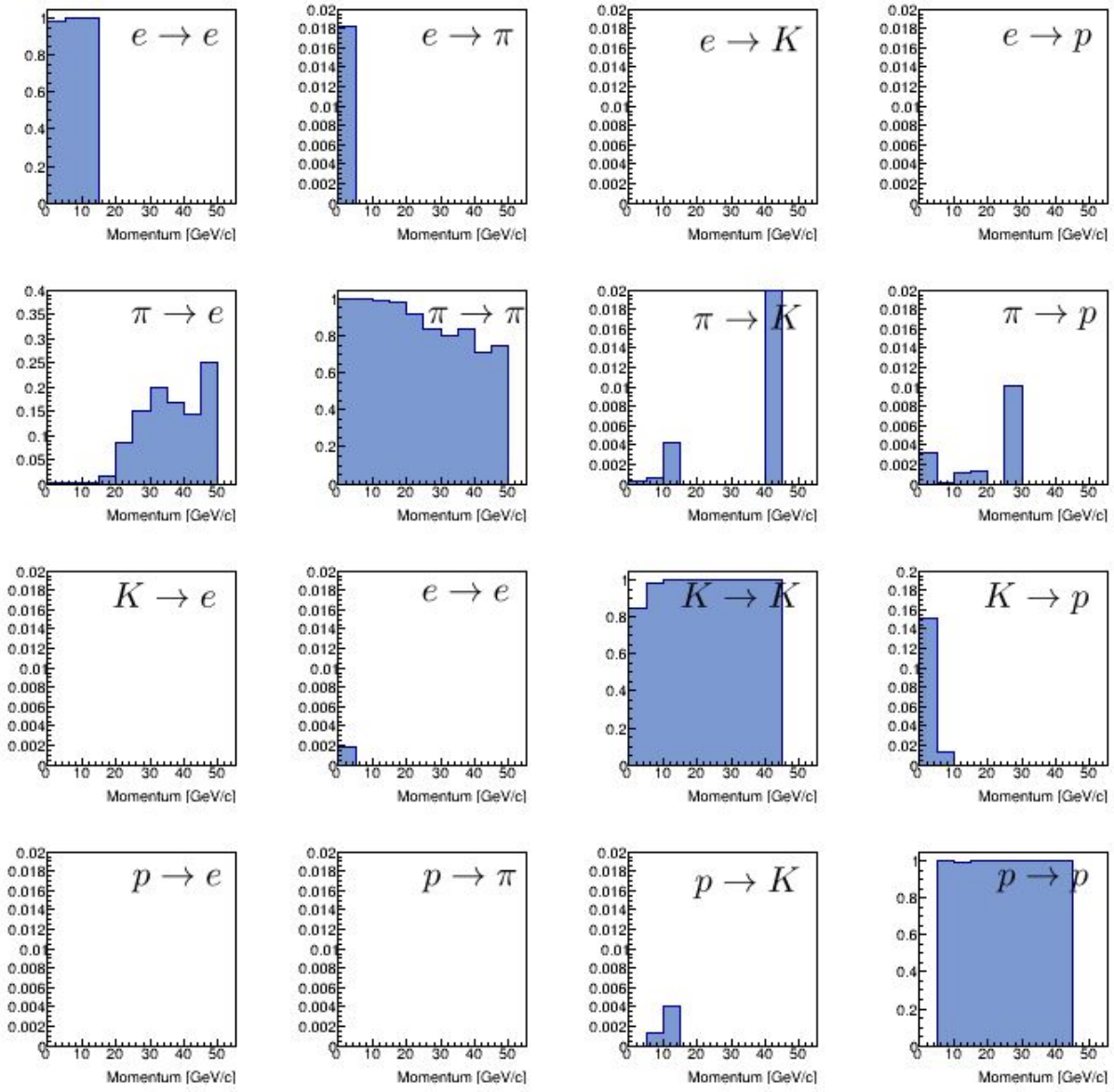


Figure 2.2.2: Particle identification performance evaluated using relative particle populations generated by PYTHIA, which resembles a typical SIDIS experiment. The Y axis shows the probability that particle of type *A* is identified as particle of type *B* according to the label *A*→*B*. Note that the identification is excellent for all the hadron species over the full momentum range, with a smooth match between the two radiators. The results are presented up to the maximum momentum analyzable within the current generated statistics. Note that while the *e*/*π* identification starts to degrade at the pion threshold of 15 GeV/*c*, the dRICH is only intended to be used in combination with the EM calorimeter, which by itself will provide a pion suppression of about 1:100 for all particle momenta.

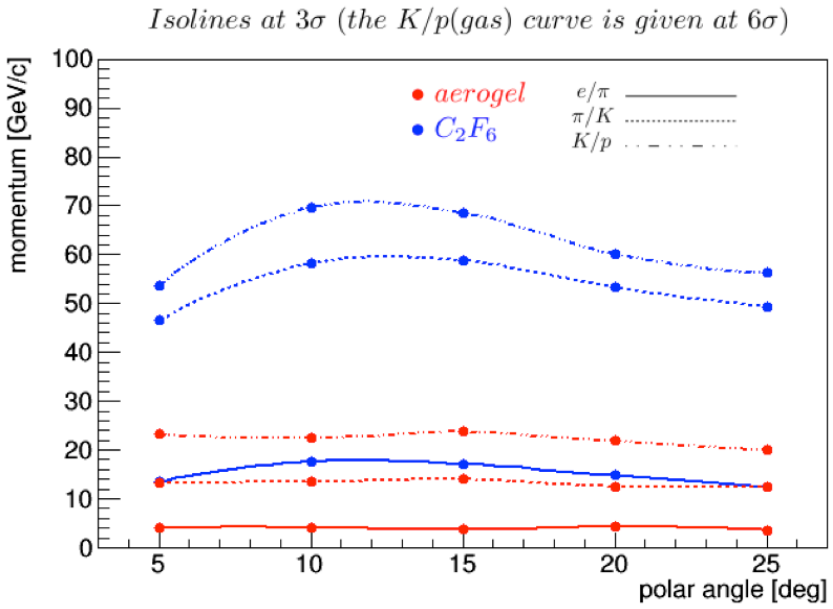


Figure 2.2.3: Momentum and angular extension of the PID at 3-sigma (and 6-sigma) level, for the aerogel and the gas (C_2F_6) radiators. The threshold momenta for the two radiators and the 4 particles are reported in Table 2.2.1.

	Nominal Momentum Threshold	
Particle	Aerogel (n=1.02)	Gas (C_2F_6, n=1.0008)
	(GeV/*c*)	(GeV/*c*)
e	0.003	0.013
π	0.694	3.49
K	2.46	12.3
p	4.67	23.5

Table 2.2.1: Momentum threshold for each particle of the considered radiators; (the refractive indices are evaluated at a wavelength of about 300 nm).

In particular, the performance of both **radiators** will need more detailed assessment:

1. Aerogel: the dRICH inherits the successful HERMES dual radiator RICH concept. However, in the HERMES RICH the intrinsic aerogel properties contributing to the angular resolution (refractive index dispersion relation, uniformity, forward and Rayleigh scattering) did not represent the main contribution to the angular error, while in the dRICH, the aerogel chromatic error (and possibly the other effects) is a dominant contribution to the angular resolution in the

lower part of the momentum range. Thus, the aerogel in the dRICH must have excellent properties (transparency, uniformity of the refractive index and number of Cherenkov photons). Aerogel producer(s)/provider(s) could be an issue, as well as aerogel properties; recent data from BLAST/Matsushita (the aerogel used in JLab/SHMS threshold Cherenkov detector [Hor17]) exist but they strongly depend on the aerogel provider (and relative production method). Long term stability and interplay with gas(es) need to be properly addressed by experimental evaluation; this may eventually require repeated and extended basic measurements. However, perhaps more importantly, it is important to study the interface of the aerogel and gas, as it is quite likely that a lack of attention to this issue led to a deterioration of the aerogel properties in LHCb. This effort will require a prototype. The characterization of the original, new, aerogel and the aerogel from the prototype can be done with minimal overhead.

2. Gas: the main candidate for the dRICH is C_2F_6 which overlaps with the aerogel before saturation of the latter and at the same time extends separation up to more than 50 GeV/*c*. There are various literature/information resources on fluorocarbons but these are relatively poor and not really up to date for C_2F_6 [Hor17, Chr99]. The number of Cherenkov photons was thus extrapolated from the existing and more copious, CF_4 data by scaling the refractive indices. As always, the scintillation level may represent a limitation and although it seems not to be a problem for visible light, it needs to be investigated further both C_2F_6 and appropriate gas mixtures. A more accurate estimate of the number of photons would also be important in the long term. Such a studies can also benefit also the eRD6 gas RICH developed for ePHENIX - although the requirements on scintillation and transparency at the very shortest wavelengths are more stringent in this case..

The **photon detector** is another critical component of the dRICH. Current single-photon detectors (MultiAnode PMTs and MCP PMTs) are rather expensive and sensitive to both the magnitude and orientation of the magnetic field. SiPMs represent a potential low-cost alternative that can operate in a magnetic fields. The compactness can also help to adapt arrays of SiPMs to the optimal curved active surface of the dRICH. SiPMs are sensitive to a single photons, but currently need to be adequately cooled and thermally stabilized. Thus, the best trade off between complexity and effectiveness of cooling needs to be explored. Radiation damage (especially from neutral particles) also represents a significant issue that needs to be considered, and a proper temperature control (cooling, annealing) can be beneficial also for this purpose. However, this can be less critical for dRICH than other detectors that are located closer to the beam pipe. Low-cost MCP-PMTs such as the LAPPDs could be the preferred solution if the sensors on the focal plane can be aligned with the magnetic field to fall within their tolerances. Since we do not yet know the final limitations, it is important to explore the possibilities of using SiPMs for the dRICH.

dRICH prototype

A prototype is necessary for the assessment the performance of the two radiators, and optimizing their interface. It will also give an opportunity to investigate the possibilities to optimize the focal plane geometry to reduce the aberrations from the spherical mirror while using a realistic set of photosensors. In order to achieve this, a preliminary configuration of the prototype has been defined, taking into account that the prototype must:

- mimic the properties and performance of the proposed dRICH components, and/or permit to derive them in a direct way.
- be cost effective (trade-off of small scale, flexibility and measurable quantities).

The prototype vessel is a 1m long cylinder with a radius of 0.3 m. This geometry is the result of the following two considerations:

- reasonable (order of 10) photoelectrons for the gas ring per particle; this number depends almost linearly on the length of the gas and therefore of the vessel.

- one needs to catch a significant fraction of the aerogel ring (20cm radius) in order to estimate the angular resolution; this constraints the transverse size of the vessel.

The minimum surface of the photon detector should be around 8x8 cm^2 to guarantees an almost 100% coverage of the gas ring (radius of approx. 4 cm), since this has a lower photon yield; a photosensor pixel size of 3 mm will keep the angular digitization (or pixel) error comparable to or smaller than the other errors, which is important for the assessment of the intrinsic sources of uncertainties from the aerogel, and will reduce multiple photoelectrons in a single pixel for the gas ring (which will help to more accurately estimate the number of Cherenkov photons). The prototype will use a small spherical mirror with 2 m radius, a support (isolated from the gas) for the aerogel tiles, and a tiny slab of UV light filter (e.g. Lucite). The proposed, preliminary prototype configuration has been modeled and simulated in GEMC/Geant4. An example of a simulated event is shown in Fig. 2.2.4 and Fig. 2.2.5.

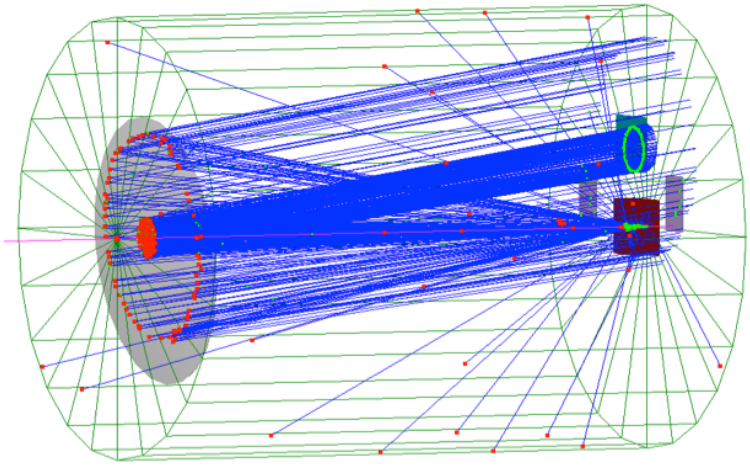


Figure 2.2.4: Simulation of a single event (with momentum above the aerogel and gas thresholds) in the dRICH proposed prototype (1 m length, 0.3 m radius). The particle travels from right to left. The Cherenkov photons produced in the aerogel (dark red) and gas all along the cylinder are reflected by the spherical mirror toward the photon detector.

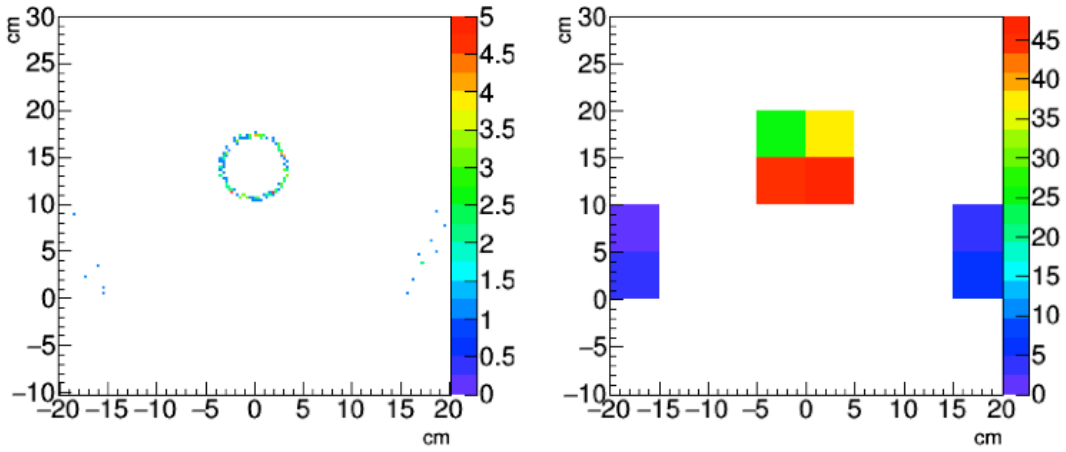


Figure 2.2.5: The simulated hits of Cherenkov photons on the photodetectors: the whole small gas ring can be reconstructed by four 5x5 cm^2 SiPM matrices, while only two opposite small arcs of the aerogel ring can be covered by the same detectors (when they are in a different configuration).

The main sources of uncertainty contributing to the 1 p.e. angular resolution have been estimated in the simulation and are reported in Table 2.2.2. It is evident how the aerogel chromatic error (and possibly forward and Rayleigh scatterings) is a relevant parameter that needs to be accurately investigated. According to the simulation, the expected number of p.e. per ring in the gas is about 14, which corresponds to 3-4 p.e. on a 5x5 cm^2 SiPM, while for the aerogel the expected number of p.e. on a single SiPM is about 0.8. Therefore, while the ring can be reconstructed on a single-event basis for the gas, cumulated events must be considered in the aerogel measurement with design thickness. Larger thicknesses could still be considered to increase the yield at the cost of a reduced emission point precision.

Table 2.2.2: Main sources of uncertainty of the single photoelectron angular resolution.

1 p.e. Error (mrad)	Aerogel	C_2F_6 Gas
Chromatic	3.7	0.9
Emission	0.2	0.9
Pixel (3 mm)	0.9	1.0

The goal of the prototype is to confirm and validate the dual radiator approach to cover the few GeV/*c* – multi tens of GeV/*c* momentum range. Moreover, critical aerogel parameters, such as the number of photons and angular uncertainties, will be explored and also possibly for different aerogel thicknesses and wavelength filters between the two radiators.

The dRICH prototype will exploit all the synergies with the mRICH activities: photosensors (MAPMTs, SiPMs) and front-end readout and DAQ will be shared between the two prototypes. At the same time, the investigation of the gas performance will be also useful to consolidate the BNL gas RICH approach.

The minimal budget for the dRICH prototype consists of the mechanical tank, the gas and related issues (one gas cylinder/2000 USD is expected to last for a single run; proper recirculation is required for safety/environmental reasons), the mirror, sensor supports, and UV filters.

The INFN manpower assigned to the mRICH activity will also be leading the dRICH prototype realization.

Aerogel (possibly), photon detectors, and electronics will be the same as for the mRICH. Depending on possible synergies with outside activities (such as CLAS12) and the capability to obtain necessary materials (*i.e.*, front-end electronics, DAQ), the FY19 dRICH prototyping activities can range from testing key concepts as part of the mRICH activity, to a full realization of the dRICH prototype, which could then be tested in parallel with the mRICH.

2.2.2 FY18 Progresses and Achievements

1. The baseline definition of the dRICH has been completed and performances investigated in details with a realistic Monte Carlo simulation based on GEMC/Geant4; feasible curved layouts of the active photon-detector surface have been investigated and optimized to minimize mirror aberrations.
2. The PID performances of the dRICH have been studied in the context of a physics channel of interest for the EIC (*i.e.*, SIDIS); as shown in Fig. 2.2.2 the result is in agreement with the expected performance.
3. A shorter version of the dRICH, adapted for the ePHENIX detector configuration has been implemented in GEMC; the evaluated performances provide interesting results even with a gas tank of 1 m. The results have been presented in the last report.
4. The dRICH analysis framework has been adapted to investigate the eRD6 gas RICH performances. The results have been presented in the last report.
5. An event-based inverted Ray Tracing approach has been initiated.

2.2.3 Proposed dRICH R&D Activities

FY19:

1. Development of a small scale, flexible, prototype that can host: aerogel, gas, mirror and either a matrix of SiPM or possibly other photon detector candidates (included the ones suitable for the only gas option like GEM).
2. Study of the interface between gas and aerogel
3. Consolidate design and test a SiPM detector matrix with proper cooling and thermal stability that needs to be designed and properly evaluated.

FY20:

1. Perform aerogel/gas characterization tests and possibly beam test measurements (better if also magnetic field is available).
2. Improve software model based on the test results and re-estimate expected performances (Tune relevant parameters used in the MonteCarlo to carry on the past years analysis/development and consolidate the performances of the proposed detectors).

2.2.4 dRICH R&D Deliverables

FY19:

1. Paper on Invert Ray tracing approach.
2. Detailed design of the dRICH prototype and its implementation.
3. First tests on SiPM + readout, in order to be ready for the beam test.

References

[Hor17] T. Horn et al., "The Aerogel Cherenkov Detector for the SHMS magnetic spectrometer in Hall C at Jefferson Lab", Nucl. Instrum. Meth.A 842 (2017) 28-47 (arXiv:1607.05264).

[Chr99] L.G. Christophorou and J.K. Olthoff, "Electron Interactions With Plasma Processing Gases: An Update for CF4, CHF3, C2F6, and C3F8", Journal of Physical and Chemical Reference Data **28**, 967 (1999).

[Ger95] R. Gernhauser et al, Nucl. Instrum. Meth.A 371 (1996) 300-304.

2.3 Modular Aerogel RICH (mRICH)

Contacts: X. He <xhe@gsu.edu>, M.Contalbrigo <mcontalb@fe.infn.it>

The state-of-the-art designs of imaging Cherenkov detectors, such as proximity focusing detectors[2], or mirror-based imaging detectors[3] require substantial volumes to be able to identify particles with momentum close to 10 GeV/*c*, due to the requirements imposed by the optical elements in the case of mirror-based detectors, or the desired ring separation in the case of proximity focusing devices. In the endcap regions of the proposed EIC detector, such space is not available. A more compact and modular design is required to fit into the available space and to still provide hadron PID capability with momentum coverage from 3 GeV/*c* to 10 GeV/*c* and *e*/ separation at lower momenta below 2 GeV/*c*.

The mRICH consists of four components. A block of aerogel serves as the Cherenkov radiator. Immediately following is an acrylic Fresnel lens, which focuses the ring image and acts as a UV filter[4]. A pixelated optical sensor is located in the image plane, and the gap between the lens and the image plane is bounded by four flat mirrors. The device is shown in Fig. 2.3.1 (left). Also shown in Fig. 2.3.1 (right) is an event display of a 9 GeV/*c* pion traveling toward the center of the mRICH detector using the Geant4-based GEMC simulation framework.

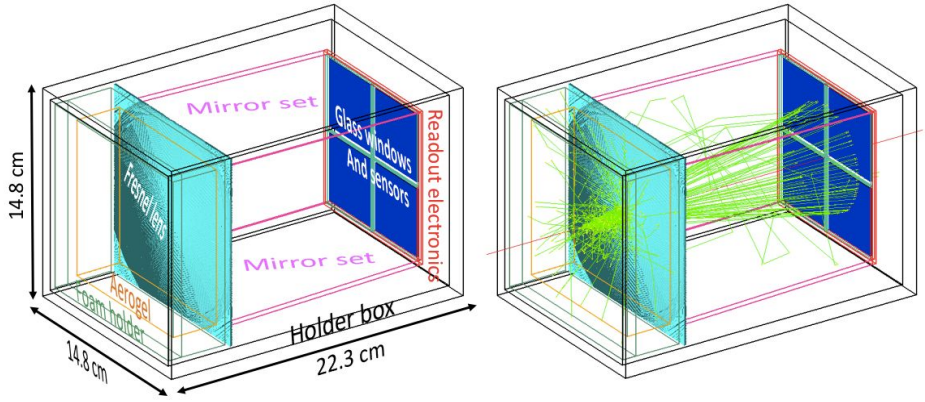


Figure 2.3.1: Left: The mRICH detector layout and its components. **Right:** An event display of a single 9 GeV/*c* pion traveling toward the center of the mRICH detector.

2.3.1 FY18 Progress and Achievements

In FY18, the main activities include: (1) the construction of the second mRICH prototype and the preparation for the second mRICH beam test at Fermilab in June of 2018; (2) the implementation of the

[2] E. Torassa, Nucl. Instr.. Meth. **A824**, 152 (2016).
M. Tabata et al., Nucl. Instr.. Meth. **A766**, 212 (2014).
[3] M. Adinolfi et al., Eur. Phys. J. **C73**, 2431 (2013).
A. Augusto Alves Jr et al., J. Instrum. **3**, s08005 (2008).
J. Engelfried et al., Nucl. Instr.. Meth. **A502**, 285 (2003).
J. Engelfried et al., Nucl. Instr.. Meth. **A431**, 53 (1999).
M. Contalbrigo et al., Nucl. Instr.. Meth. **A639**, 302 (2011).
R. A. Montgomery, Nucl. Instr.. Meth. **A732**, 366 (2013).
[4] D.E. Fields et al., Nucl. Instr.. Meth. **A349**, 431 (1994).

mRICH detector in the Forward sPHENIX experiment; (3) the study of the mRICH performance in the EIC detector designs using Pythia events.

Second mRICH Prototype

The new mRICH prototype has been built at Georgia State University (GSU) based on the successful first beam test of the first prototype. The key changes in this prototype (see Fig. 2.3.2) include: (1) separation of the optical components from the readout electronics for easy integration and to avoid overheating the electronics; (2) a longer focal-length (6") Fresnel lens; (3) use of four multi-anode PMT arrays (H13700-03, 3mm x 3mm pixel size) from Hamamatsu; and (4) use of aluminum panels for the detector frame instead of acrylic sheets to shield the external ambient light.

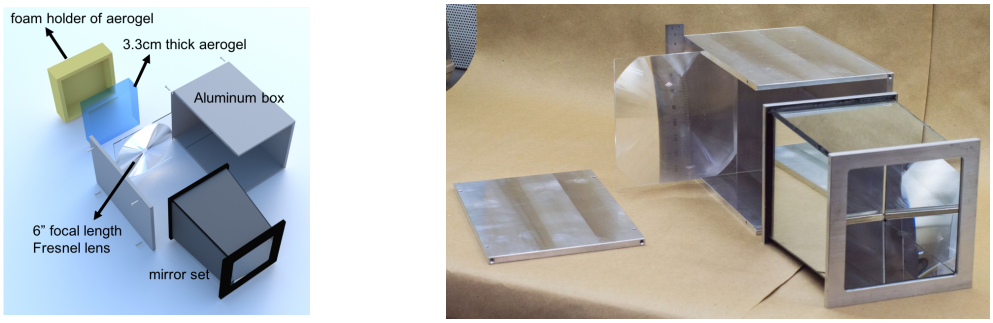


Figure 2.3.2: Left: 3D rendering of the second mRICH prototype. **Right:** The second mRICH prototype under construction.

In order to explore other lens options, we constructed two new mRICH prototypes. One is using Fresnel lens and the other is using a spherical lens, as shown in the left picture of Fig. 2.3.3. Figure 2.3.3 also shows the test stand with the beam hodoscope. The fully populated beam hodoscope is shown in Fig. 2.3.4. The dimension of the finger scintillator is 10mm x 10mm x 200mm. The readout for the second mRICH beam test is being jointly provided by the INFN and the Hawaii University groups.

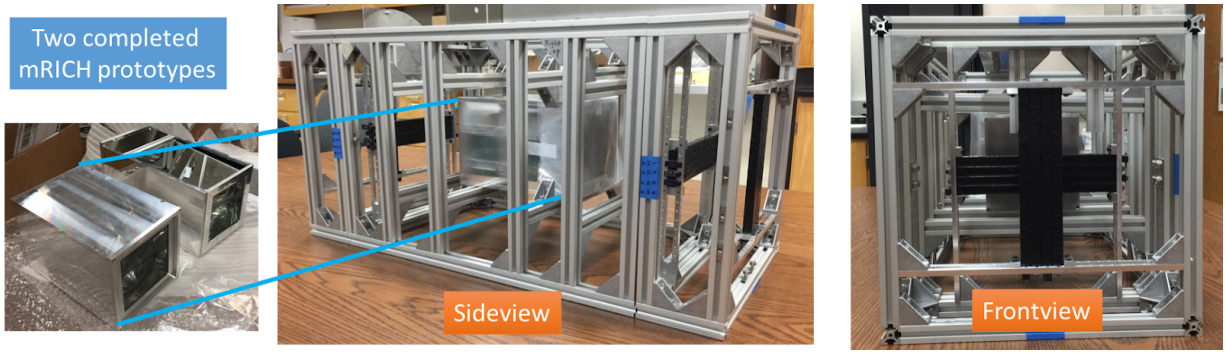


Figure 2.3.3: The completed mRICH test stand for a single-module test. The left picture shows the two mRICH prototypes (one with Fresnel lens, and the other with a spherical lens); the middle picture shows a side view of the test stand; the right picture shows the front view with a partial installation of the finger hodoscope.

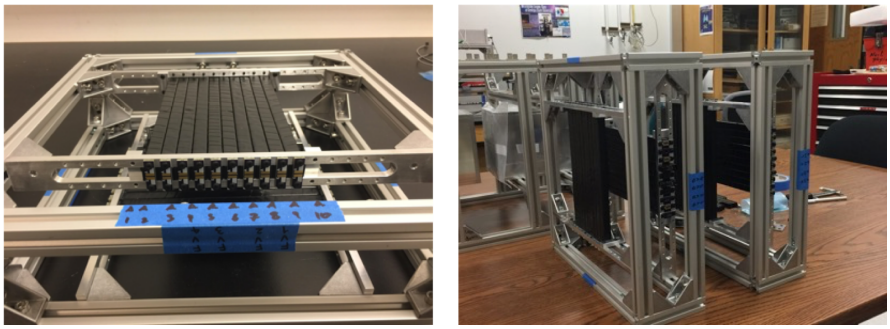


Figure 2.3.4: A pair of fully populated beam hodoscopes to be used for the second beam test at Fermilab in June 2018. There are 10 finger scintillators in each direction in order to cover the secondary beam particle spread, which is about 10-cm wide.

mRICH in the Forward sPHENIX Experiment

In order to validate the mRICH detector PID performance in real experiments before EIC coming online, an implementation of the mRICH detector array in the Forward sPHENIX has been proposed in a recent Letter of Intent to BNL (as shown in Fig. 2.3.5). The addition of the mRICH detector to the Forward sPHENIX will not only enhance the physics capabilities of the sPHENIX experiment but will also make the sPHENIX detector a realistic detector for future EIC experiments. The mRICH implementation in the forward region is the first step of upgrading sPHENIX with PID capability.

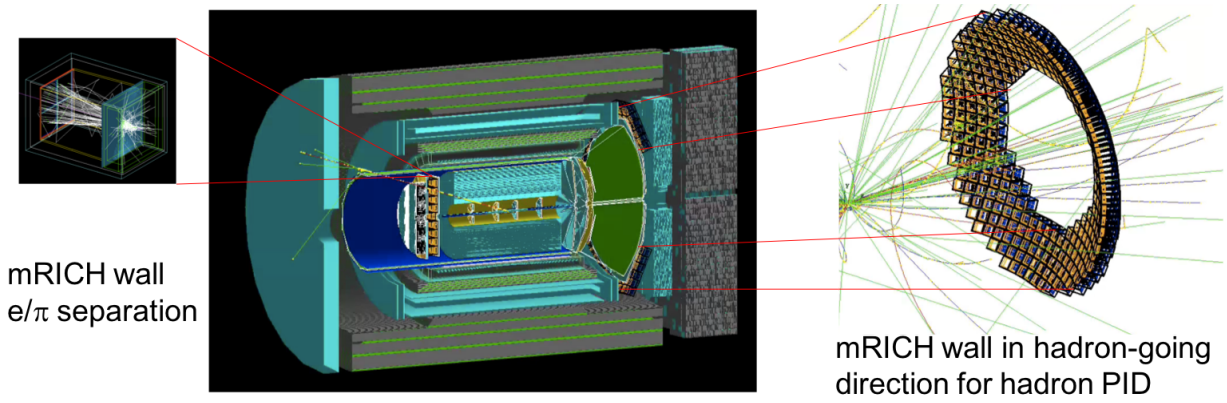


Figure 2.3.5: Conceptual design of the Forward sPHENIX with the mRICH detector arrays.

Xu Sun (a post-doc at GSU), together with Zhiwen Zhao (Duke University), is leading the development of PID algorithms with mRICH using a log likelihood method. As an example, Fig. 2.3.6 shows ring-image patterns that have been generated in a realistic Geant4 simulation by 5-GeV/*c* pions, kaons, and protons. A systematic study of this PID method is currently ongoing.

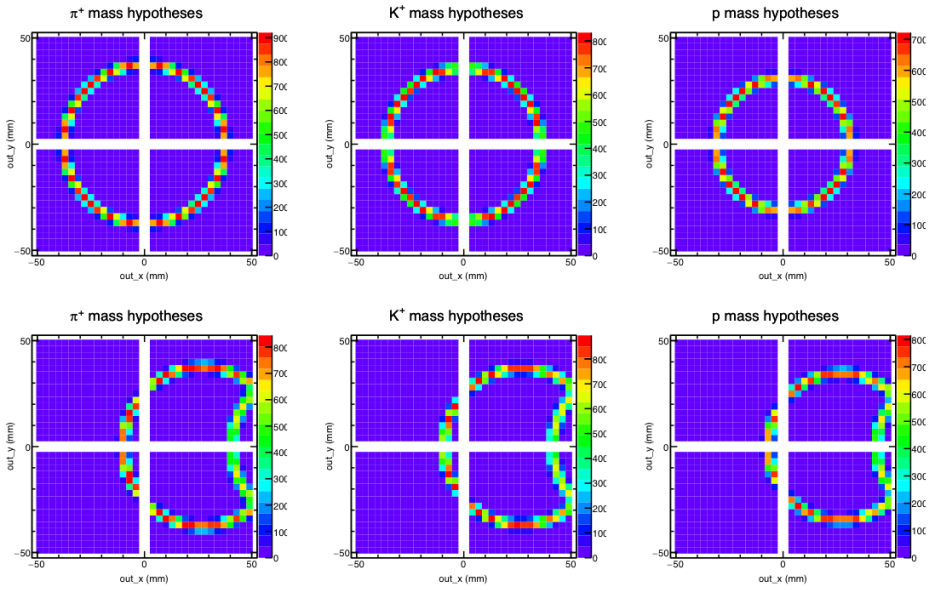


Figure 2.3.6: Cherenkov ring-image patterns generated in a Geant4 simulation. A log likelihood method uses these patterns to provide the PID information. The top row shows the image patterns from pions, kaons, and protons at 5 GeV/*c*. These particles enter perpendicularly to the front of the mRICH module at the center. The bottom row shows the image patterns when the particles enter at an angle of 10°.

2.3.2 Proposed mRICH R&D Activities

In FY19, the proposed activities aim to finish the data analysis of the second mRICH beam test and to publish the results, as well as to perform other planned mRICH R&D tasks. In parallel, a joint beam test with the dRICH prototype will be organized to focus on the design readout chain connecting the new front-end chip (TARGETX/SIREAD) and the SSP protocol. Such a beam test will also provide the chance to continue the detailed study of the mRICH optical performance. Specifically, we will work on

- Data analysis of the second mRICH beam test.
- Study of the radiation hardness of the Fresnel lens.
- Development of an optical characterization system to measure the lens and aerogel block properties.
- Simulation study of mRICH performance in the Forward sPHENIX experiment at BNL (ongoing effort).
- Simulation study of mRICH performance in the electron endcap of JLEIC (ongoing effort).
- Organize a joint dRICH/mRICH beam test.

2.3.3 mRICH R&D Deliverables

FY19:

- Publication of the results of the second beam test of the mRICH prototype.
- Report on the performance of mRICH array in EIC-like experiments.
- Report on the results of a detailed study of the radiation hardness of the Fresnel lens.

2.4 DIRC

Contacts: G. Kalicy <gkalicy@jlab.org>, J. Schwiening <J.Schwiening@gsi.de>

A radially-compact detector based on the DIRC (Detection of Internally Reflected Cherenkov light) principle, shown in Fig 2.4.1a, is a very attractive solution for EIC, providing particle identification (e/π, π/K, K/p) over a wide momentum range. The DIRC detector is a special kind of RICH counter using rectangular-shaped radiators made of synthetic fused silica that are utilized also as light guides to transport Cherenkov photons to an expansion volume, where the photons are recorded by an array of photon sensors. During the photon transport, the emission angle of Cherenkov photons with respect to the particle track is maintained and can be reconstructed from the measured 3D parameters: the image location on the detector surface (x, y) and the time of arrival of each photon (t).

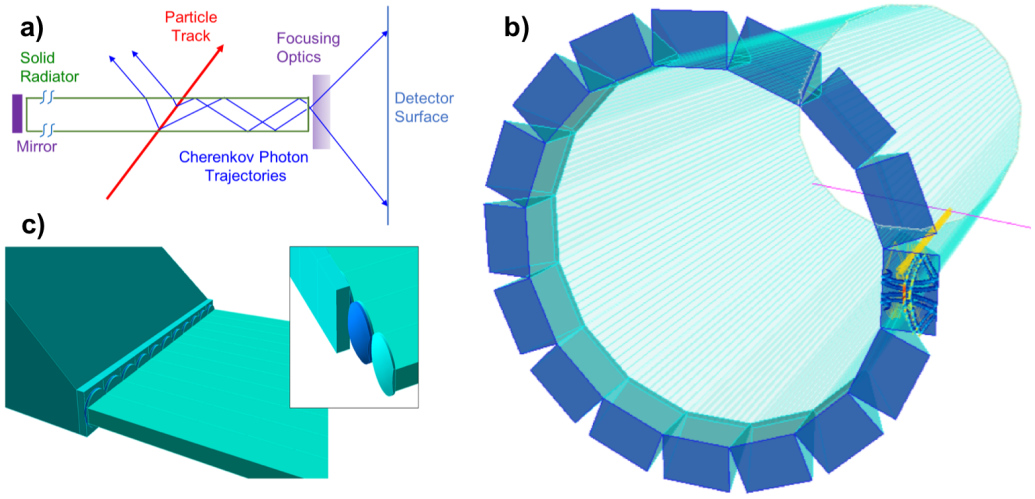


Figure 2.4.1: a) Schematic of the DIRC principle. b) Geant4 geometry for the simulation of the High-Performance DIRC where one can see the accumulated Cherenkov photon hit pattern from a single charged kaon. c) The fused silica prism expansion volume, a row of spherical three-layer lenses with high index of refraction (no air gaps) and the radiator bars. The insert shows the individual lenses and layers of the spherical lens system.

2.4.1 Summary

The objective of the DIRC R&D undertaken by the EIC PID consortium is to extend the PID capabilities of DIRC counters well beyond the state-of-the-art. The past R&D activities funded by this program (initially eRD4, later eRD14) demonstrated the feasibility of a high-performance DIRC to provide 3σ separation of π/K up to 6 GeV/c, e/K up to 6 GeV/c, e/π up to 1.7 GeV/c, and K/p up to 10 GeV/c. The implementation of the High-Performance DIRC into a Geant4 simulation is shown in Fig. 2.4.1b. Key elements in achieving this performance are innovative focusing optics (visible in Fig 2.4.1c) and time-based reconstruction algorithms. The ultimate goal of the ongoing program is to demonstrate this performance in a test beam with a prototype that is representative of the intended EIC configuration

(small-pixel photosensors, high-resolution timing, advanced optics, *etc.*). Milestones towards achieving this goal include the design, characterization, and validation of a radiation-hard lens as well as the detailed simulation of the High-Performance DIRC design and the development of the reconstruction algorithms. The last phase of the project will involve the validation of the simulated performance of the High-Performance DIRC design with the full system prototype in particle beams.

In the past fiscal year our major activities were (1) evaluation of the performance of the cylindrical 3-layer-lens prototype procured in FY17 and (2) identification of radiation hard materials for the next lens prototypes. The optical properties and performance of the cylindrical lens were measured in a test lab and with a particle beam, respectively, and were found to be in excellent agreement with the simulated ones. We identified two very promising radiation hard materials to replace the NLaK33 glass: PbF_2 and sapphire. The initial simulation studies of the High-Performance DIRC with both materials suggest similar/improved PID performance. Measurements of these new materials, such as a radiation hardness test with the ^{60}Co source, are in progress.

The EIC DIRC R&D program has been greatly benefiting from a synergy with the PANDA DIRC R&D program, which has involved know-how, hardware, and software contributions. A key future component of the EIC DIRC program will be the transfer of the PANDA Barrel DIRC prototype to the U.S., which reflects the long-term interest of the GSI DIRC group to remain involved in the EIC project.

2.4.2 FY18 Progress and Achievements

The focus of our activities in FY18, as recommended by the committee, was on the investigation of radiation-hard materials for the 3-layer lens, the evaluation of the performance of the cylindrical 3-layer lens prototype, and the preparation for the next lens prototype. The outcomes of these activities include the confirmation of critical parameters of the lens, in particular the flat shape of its focal plane. The cylindrical 3-layer lens also performed well in the PANDA Barrel DIRC prototype during tests with particle beams. Two promising candidates for the radiation-hard alternatives to NLaK33, used as a middle layer of the lens, were identified. Simulation studies of the High-Performance DIRC demonstrated that both materials are capable of reaching the required PID performance. Experimental studies of the candidate materials are being prepared.

Identification of Radiation-Hard Materials for the Next Lens Prototypes:

Radiation Hardness Measurement of NLaK33 with X Rays

We completed the NLaK33 radiation hardness study with X-Rays (started in FY17) by increasing the accumulated dose. The size of the irradiated sample was 28x8x8 mm, which means it is four times thicker than the expected middle layer of lens. The measurement showed a significant loss of transmission after exposure to a 6 krad dose (see Fig. 2.4.2). Most of this loss was recovered through annealing at a room temperature. A study of the healing process showed that, at 420 nm, 3–4% of transmission are recovered

during the first 24 hours and that the recovery rate slows down after that. The radiation hardness characterization of NLaK33 will be concluded by exposing it to gamma rays as described below.

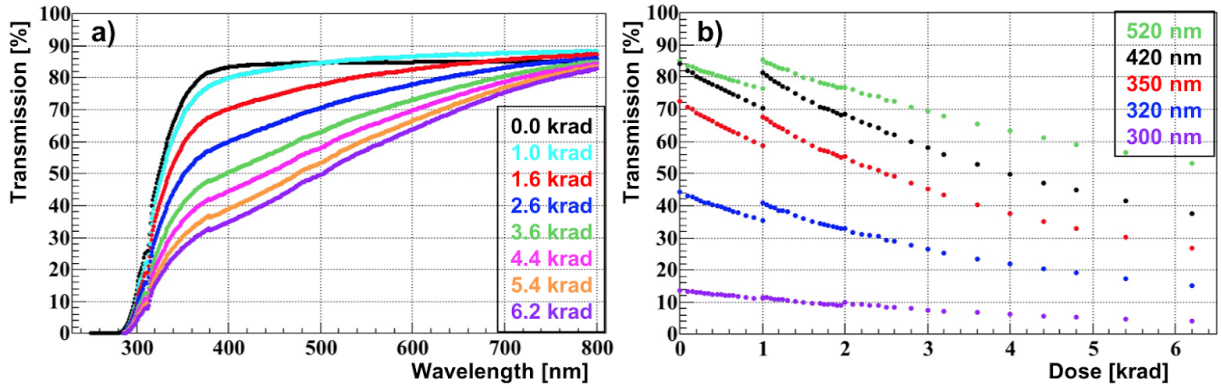


Figure 2.4.2: Measured transmission (not corrected for Fresnel losses) through the 8mm thick NLaK33 sample as a function of wavelength for selected amounts of deposited X-ray dose (a) and as a function of X-ray dose for selected wavelengths (b).

Radiation Hardness Measurement with ^{60}Co

A commonly used source for studies of radiation hardness of optical materials is ^{60}Co. Following the July-2017 and the January-2018 recommendations by the R&D review committee, we have started the preparation for radiation-hardness measurements with ^{60}Co. We have secured a window of opportunity to carry out these measurements in August 2018 at no cost at the BNL radiation facility. We plan to irradiate several lens-candidate materials, namely PbF_2 and sapphire, as well as NLaK33, to accumulated doses of 100 krad and higher. In addition, we will irradiate the acrylic Fresnel lens currently used for the mRICH prototype.

We will analyze the collected data during the last two months of FY18. Based on past experience, we anticipate that a follow-up radiation-hardness measurement, with an extended dose range and possible evaluation of radio-luminescence, will be needed in FY19.

Simulation of the High-Performance DIRC with Radiation-Hard Material

The assessment of the PID performance of DIRC with radiation-hard optical materials is an important aspect of the selection of a suitable lens material. Lenses with PbF_2 and sapphire as the middle-layer material were implemented in the High-Performance DIRC Geant4 simulation. Figure 2.4.3 shows the evaluated π/K separation power and the photon yields for 6 GeV/c particles for both, PbF_2 and sapphire, compared to those for NLaK33.

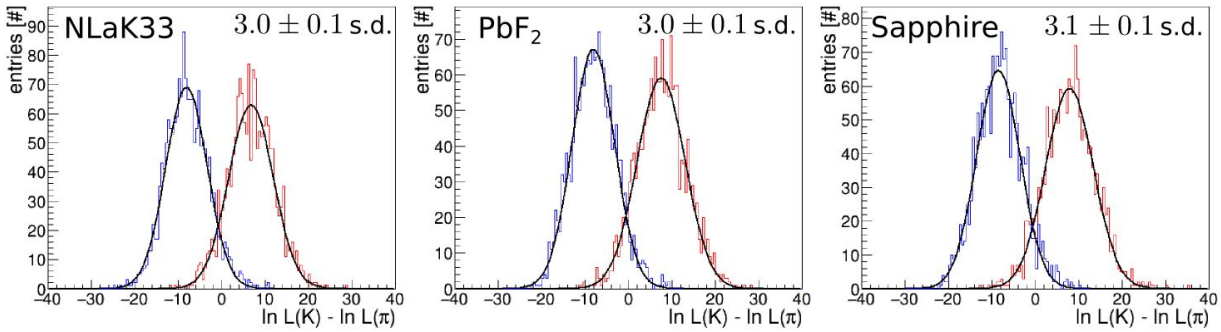


Figure 2.4.3: Comparison of the simulated High-Performance DIRC performance with three possible materials for the middle layer of the 3-layer lens: NLaK33, PbF_2, and Sapphire. π/K separation for charged pions and kaons with 6 GeV/c momentum and 30° polar angle, assuming a tracking resolution of 0.5 mrad.

Performance Evaluation of the Cylindrical 3-Layer-Lens Prototype Procured in FY17:

Results of the FY18 data analysis of the last test beam at CERN

The analysis of the data collected with the PANDA Barrel DIRC during the test beam at CERN in August/September 2017 was primarily focused on the validation of the PID performance of two optics configurations (a) a narrow bar with the 3-layer cylindrical lens and (b) a wide radiator plate with the 3-layer cylindrical lens. Photographs of the lens and the geometry (b) used in test setup at CERN are

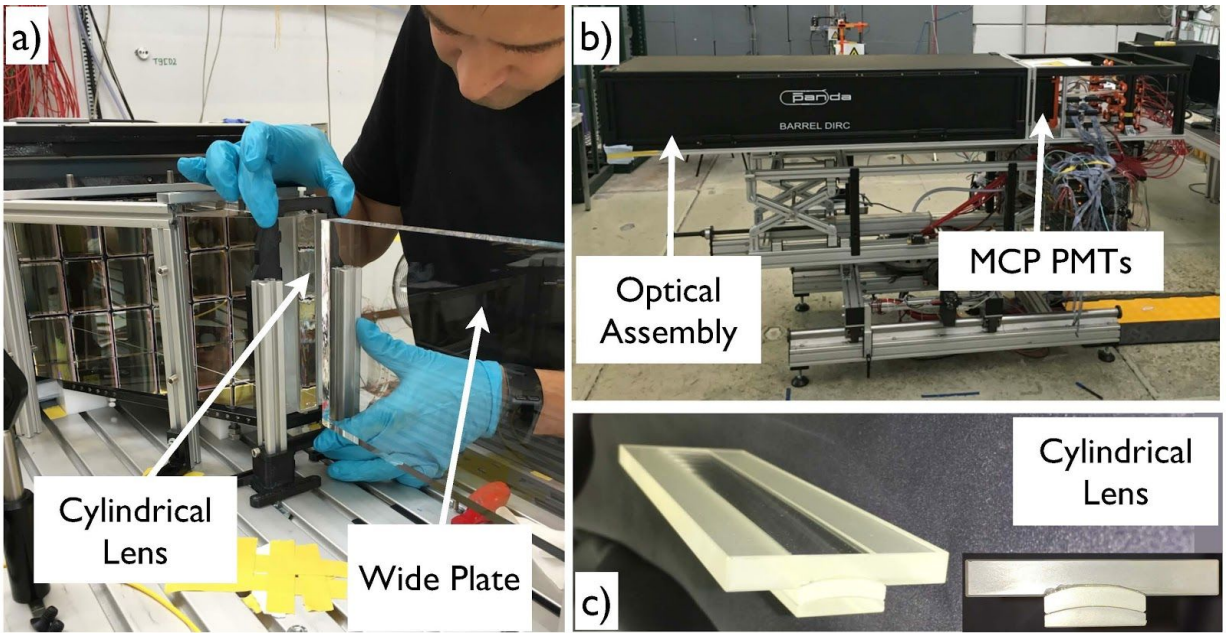


Figure 2.4.4: a) A photograph of the lens coupled to a wide plate and installed in the PANDA Barrel DIRC 2017 prototype at CERN; b) The PANDA Barrel DIRC prototype setup at CERN; c) A close-up photo of the cylindrical lens. The right bottom photo shows a cross section of the lens where one can clearly see the 3-layer structure.

shown in Fig. 2.4.4. The radiator (plate or bar) was coupled to the 3-layer cylindrical lens, which was

connected directly to the synthetic fused silica prism expansion volume with a 33° opening angle.

The performance of the wide plate geometry with the cylindrical 3-layer lens is shown on Fig. 2.4.5. One should remember that the measurement is performed with a setup testing the PANDA DIRC configuration. The separation power for the EIC DIRC detector is expected to be much better due to smaller pixel size of the photodetector and improved time resolution. However, the very good agreement between the experimental and the simulated data is important for the EIC R&D program. The same simulation package that was used in this analysis was also used to simulate the performance of the High-Performance DIRC detector.

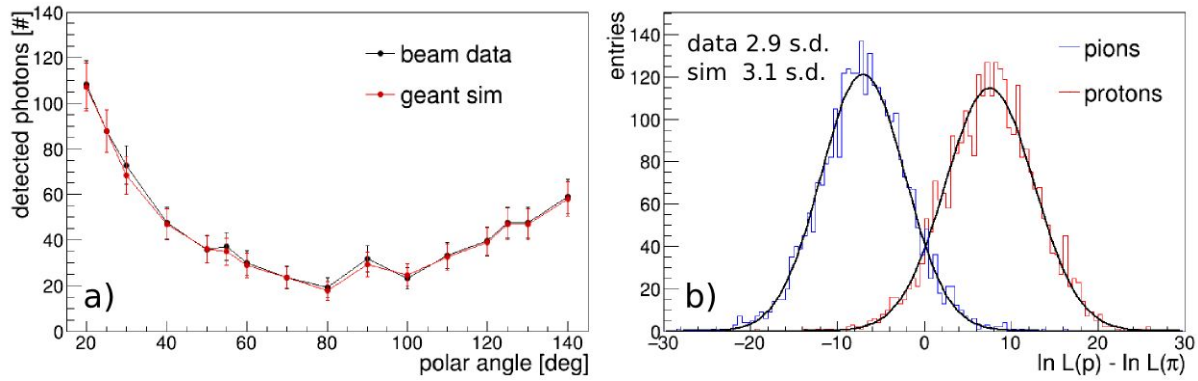


Figure 2.4.5: Preliminary result of the PANDA Barrel DIRC prototype with the 3-layer cylindrical lens from the 2017 CERN test beam: a) photon yield for tagged protons as a function of the polar angle at a momentum of 7 GeV/c; b) π/p separation power for tagged pions and protons at a polar angle of 25° and a momentum of 7 GeV/c.

Mapping the focal plane of the 3-layer cylindrical lens

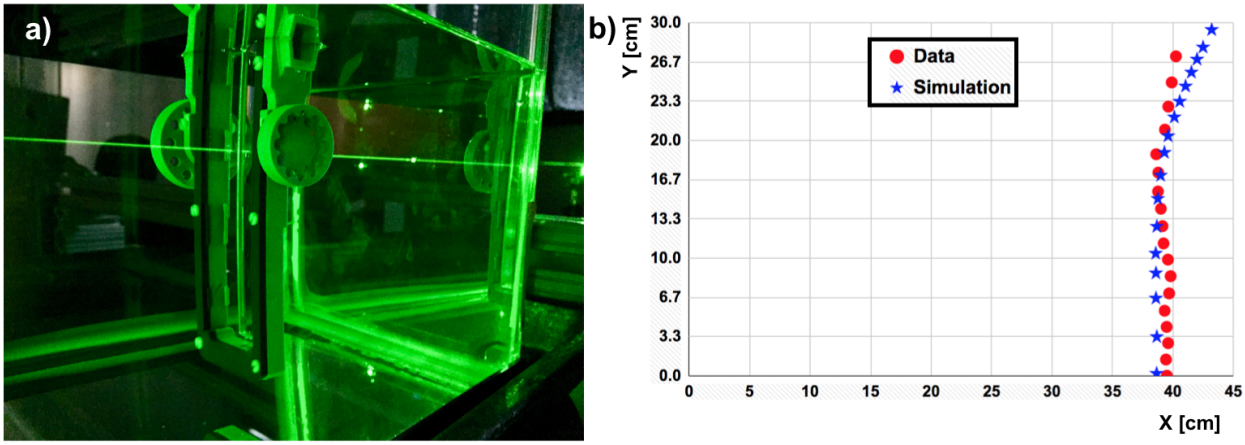


Figure 2.4.6: Measured shape of the focal plane (red points) compared to simulation (blue stars). The x coordinate corresponds to the focal length and the y coordinate to the focal point location perpendicular to the incident beams, calculated for different lens rotation polar angles.

The 3-layer cylindrical lens was placed in a setup in the Old Dominion University laser lab to measure the shape of the focal plane by rotating the lens through two parallel laser beams. The intersection point of the

two laser beams determined the focal length. The lens was placed inside a 30 x 40 x 60 cm^3 glass container filled with mineral oil (with a refractive index very close to fused silica) to simulate the focusing behavior of the lens placed between the bar and the prism. The 3-layer lens was supported by a special 3D-printed holder that made it possible to map out the focal plane in all three dimensions. The cylindrical 3-layer lens prototype in the setup with green laser shining through it is shown on Fig. 2.4.6a. The results of that measurement were compared to the predictions from the GEANT4 simulation. Figure 2.4.6b shows the result for both laser beams centered on the lens, separated by 1 mm. During this measurement, the lens was set perpendicularly to the laser beam plane (0° tilt), the lens was rotated from 0° to 34°, confirming that the measured shape of the focal plane is in good agreement with the simulation. Additional measurements for other rotation angles and off-center laser beam positions are planned. The cylindrical lens produces the desired flat shape of the focal plane for the beams close to the center of the lens.

2.4.3 Proposed DIRC R&D Activities

The production of a radiation hard 3-layer lens will be an essential step for the the High-Performance DIRC R&D process. Several new materials were identified as potential candidates for EIC DIRC during FY18. In FY19 we shift our efforts to detailed tests of the materials and the fabrication of a radiation-hard lens prototype. Based on the very promising simulation studies, PbF_2 and sapphire have become the leading candidates. Initial radiation hardness test of these materials will be performed in August 2018 using the ^{60}Co source at BNL. Later in FY19, a more detailed study is planned on birefringence as well as radio-, UV- and visible luminescence of the candidate materials. We also plan to include more candidate materials for the second test, including doped Dense Flint glasses and Cerium doped glasses.
Producing two 3-layer lens prototypes, with the middle layer made of PbF_2 and sapphire, respectively, is the main capital investment request for the DIRC@EIC group. Both materials are very challenging to machine by the optical industry (due to the toxicity of the lead and the hardness of the sapphire) and most companies do not want to work with these materials. However, we were able to identify two vendors, one in China and one the US, who are willing to build the lenses and who submitted quotes for a prototype production. We believe it is crucial not to pass on both unique opportunities.

The current High-Performance DIRC implementation in Geant is based on the properties of available commercial MCP-PMT sensors. However, the latest generation of MCP-PMTs, currently being tested for the PANDA experiment, features a significantly higher photon detection efficiency (PDE) with a useful wavelength range extended much further into the UV. Upgrading the properties of the sensors and of the glue used in the bar assembly will make use of the enhanced UV transmission offered by the sapphire in the new 3-layer lens prototype, which should improve the PID performance.

The evaluation of the optical properties of the cylindrical 3-layer lens prototype will be completed in FY19, including additional tilted lens positions and studies of the optical aberrations using off-center laser beams.We plan to combine the results of these studies with measurements taken in FY17 and FY18, for both the cylindrical and spherical prototype lenses, into a publication in NIM.

The High-Performance DIRC is an important part of all three proposed EIC central detector concepts. The increasing interest in EIC physics studies with Monte Carlo data demonstrates the need for (1) a parametrization of the High-Performance DIRC baseline performance that will be used as input to the fast EIC detector simulations and (2) the implementation of a more realistic DIRC detector design in the three full simulation frameworks. The parameterization will be useful for all three detector concepts since the differences in the geometry constraints for DIRC between them are minor. Following the initial High-Performance DIRC design implementation, it is now crucial to study the effect of different bar sizes, focusing system options, expansion volume shapes and dimensions, as well as sensor types (MCP-PMTs vs. SiPMs) and pixel sizes on the DIRC performance to identify a credible and cost-efficient baseline design for the High-Performance DIRC. The implementation of this design in the full EIC central detector simulation frameworks is an important step to facilitate the study of the combined PID performance of the eRD14 detector systems. Other important simulation activities are the study of the mitigation of chromatic dispersion effects using fast timing and the potential use of the DIRC for precise event timing.

The next step in the development of readout electronics will require fine pixel sensor soon. The only commercially available candidate is the PHOTONIS XP85122-S with a pixel pitch of 1.6 mm. However, given the current funding situation, we decided to prioritize the lens development for the FY19 and postpone the procurement of a sensor with a smaller pixel size to FY20.

Synergetic Activities Supported by External Funding

The synergy with the PANDA Barrel DIRC project not only provided access to the prototype and the CERN test beams in 2015, 2016, 2017, and 2018 but includes several planned mid- and long-term contributions from the GSI DIRC group to the EIC DIRC project. With the submission of the PANDA Barrel DIRC TDR in 2017 the activity focus of the GSI DIRC group on PANDA will shift to the mechanical design and the R&D for the detector assembly. Both activities are directly relevant to the EIC DIRC design.

After conclusion of the beam tests of the PANDA Barrel DIRC, components of the prototype are expected to become available for use by the EIC DIRC effort during FY20/FY21 on the basis of a long-term loan or an in-kind contribution. The mechanical prototype structure, as well as at least one narrow bar, one wide plate, one prism expansion volume, and a set of PHOTONIS XP85012 MCP-PMTs for initial tests, could be transported to the U.S. for prototype beam tests at JLab or Fermilab. This would significantly reduce the financial investment required to set up the first prototype for the test of lenses, sensors, and readout electronics with particle beams (this would be a deliverable in FY21/FY22). In FY18 we started to investigate the administrative process required for a loan agreement between GSI and CUA (the U.S. receiving institution). This activity will continue in FY19 with the goal of completing the transfer in FY20.

Development of the LAPPD sensors and readout are well in line with High-Performance DIRC timeline. The 32x32 channel version of this sensor will be crucial to start work on the readout electronics prior to the assembly of the complete prototype. The first step of the High-Performance DIRC prototype will be to reproduce the PANDA results in a reference measurement, using the PANDA optics and XP85012 MCP-PMTs (with 6.5mm pixel pitch). The ultimate goal is to assemble an EIC DIRC prototype with proper pixel-size sensors and appropriate geometry to validate the simulated performance and to directly measure the PID performance.

Proposed activities

FY19

- Detailed study of optical properties and radiation hardness of alternative materials for the middle layer of the 3-layer lens with X-ray, ^{60}Co, and neutron sources.
- Finalize the evaluation of the cylindrical 3-layer lens using the 2017 and 2018 CERN prototype test beam data and lasers in the optics setup.
- Designing and fabricating two 3-layer lens prototypes with PbF_2 and sapphire as middle layer.
- Implementing upgraded sensors in the High-Performance DIRC simulation.
- Cost/performance study to identify optimum bar, pixel, and expansion volume size as well as different focusing system for a future baseline design.
- Implementation of a baseline design into JLab-EIC, EIC-sPHENIX and BeAST detector simulation frameworks.
- Investigation of the potential use of DIRC for high-precision event timing.
- Investigation of chromatic dispersion mitigation in the context of different photocathode materials and readout timing precisions.

FY20

- Phase 1 of dedicated DIRC@EIC prototype development (modified PANDA DIRC prototype, possible in-kind contribution from GSI).
- Development of analytical version of time-based imaging.
- Optimization of design in coordination with the other eRD14 PID systems within full EIC central detector simulation framework.
- Study PID performance of the baseline design in the presence of backgrounds.

2.4.4 DIRC R&D Deliverables

FY19

- Detailed study of candidates for radiation hardness of candidate lens materials, including PbF_2 and sapphire, with a ^{60}Co source.
- Design and fabrication of a 3-layer lenses with improved radiation hardness using PbF_2 and sapphire.
- Implementation of the High-Performance DIRC into the JLab-EIC, BeAST, and EIC-sPHENIX detector simulation frameworks.
- Complete performance evaluation of the cylindrical 3-layer lens on test benches.
- Publication describing the performance validation of the focusing lens-based optics using the DIRC prototype in particle beams.

2.5 High-resolution Time-of-Flight (TOF)

Contacts: M. Chiu <chiu@bnl.gov>, M. Grosse-Perdekamp <mgp@uiuc.edu>

High-resolution TOF provides an attractive solution for PID covering the lower momenta range at the EIC, below the turn on threshold for gas Cherenkov detectors. The R&D pursued here intends to push the state of the art of two technologies, MCP-PMT and mRPC, with an ultimate goal of 5 and 10 ps, respectively. Assuming a total resolution of 10 ps and a distance of 1 m, TOF could achieve 3σ separation for π/K and K/p of 3.5 and 6 GeV, respectively, which would be adequate for mid-rapidity PID. In the hadron going direction, where the TOF wall could be placed 3 m from the interaction point, the 3σ separation for π/K and K/p would be 6.5 and 11 GeV. Coupled with a dE/dx measurement from a TPC, TOF would also provide electron identification up to several GeV. Besides providing PID, TOF enables bunch association which is required since each bunch may have a different polarization.

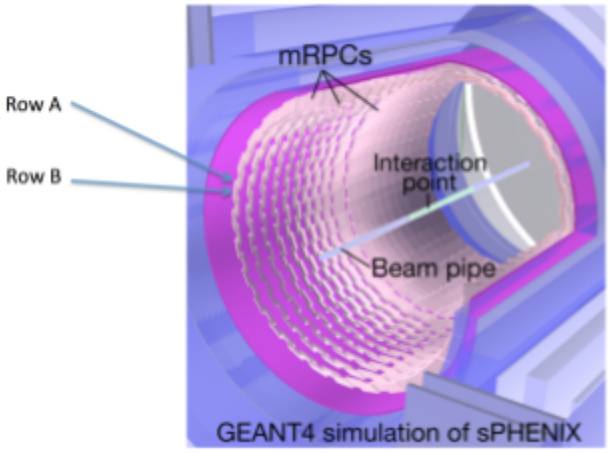


Figure 2.5.2: mRPCs implemented in the sPHENIX simulation as a barrel TOF system. The inner silicon tracking and TPC have been suppressed when drawing in order to show the projective mRPC modules.

2.5.1 FY18 Progress and Achievements

High performance TOF was funded during the past cycle at the level of $5k for CCNY, for the production of revision 2 of our custom UFAMP fast preamps. However, our group has continued some development as available resources have permitted.

Within eRD14 (and previously eRD10), our group has demonstrated that a resolution of ~20 ps is achievable with glass mRPCs by using thinner glass, making smaller gas gaps (up to some minimum level around 100 μm), and increasing the number of gaps. Our previous results confirms earlier results from C. Williams *et. al*., and is only the 2nd set of mRPCs to achieve such resolutions. To achieve even better resolution for the mRPC, we have proposed that one solution is to replace the glass with even thinner dielectrics and thus increase the number of gas gaps. We believe a mRPC with 48 gas gaps is possible in the same space as the 24 or 36 gap mRPCs from C. Williams and eRD14, respectively.

Other limits to the timing resolution may come from a dependence of the timing on the hit position of the particle on the strips. The strips are 1 cm wide, which is greater than the 10 ps equivalent of 3 mm. A tracker system is developed for use in the lab to be able to study the position dependence of the timing resolution. The major impediment to being able to do this study (and all other mRPC studies) efficiently is the lack of more scalable electronics for our testing. We currently use TI amplifier evaluation boards for preamps with the DRS4 evaluation board for digitization for a total of 4 channels. With this setup, we can only read out 1 strip on a pair of mRPCs, since we read out both ends of the strip on the two detectors.

With custom preamp boards that are designed to match the spatial constraints of the mRPC, and a custom DRS4 digitizer board, we should be able to instrument 8 or more pairs of strips, thus increasing our data-taking rate by an order of magnitude. To that end, two years ago we developed a custom preamp board built on the TI LMH5401 8 GHz amplifier, the UFAMP, which was designed to have 900 MHz analog bandwidth and a gain of ~9. We have studied the performance of the UFAMP using a network analyzer and confirmed on the bench with a fast pulser capable of 1 ps risetime edges, and determined that due to parasitic capacitances on the board the actual bandwidth is 300 MHz. Thus, a 2nd revision of the board was needed. While we lost the original designer of the UFAMP (Andrey Sukhanov) to the collider department due to budgetary issues at BNL, we have fortunately added two highly experienced groups, one led by Alexei Denisov of IHEP Protvino, and the other Bruce Kim[5] of CCNY, who is an electrical engineering professor there. They have systematically looked at the impedance of the cathode strip boards and other causes of the reflections noticed in earlier studies. We believe we understand the impedance of the board, which is complicated by the fact that there are multiple connected layers, and that in addition the reflections were exacerbated by a passive summing of the 2 or 3 strips on each channel of readout. The new revision of the preamp board will incorporate the proper impedance matching and actively sum the strips to solve these problems.

Even with the custom preamps, the DRS4 evaluation board limits the number of channels of readout to 4. An 8 channel DRS4 board, which can be run from the same clock to support as many channels of synchronized readout as needed, was designed last year by A. Sukhanov, and improved recently by A. Denisov. A block diagram of the schematic is shown in Fig. 2.5.4. With the rev2 version of the UFAMP preamps and this DRS4 board, we should be able to instrument 8 or more pairs of mRPC strips at a time, and thus vastly increase the speed of studies of the factors affecting mRPC timing performance.

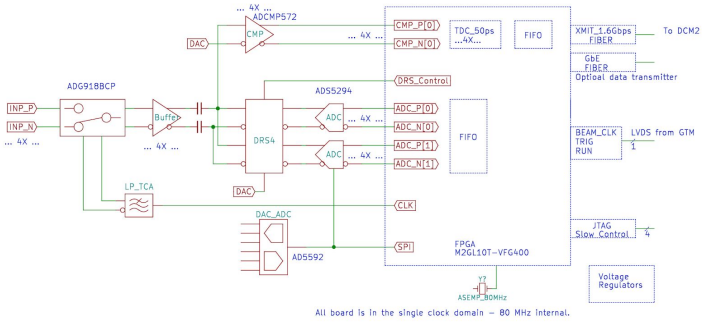


Figure 2.5.1: Block diagram for the proposed DRS4-based prototype board.

[5] https://www.ccny.cuny.edu/profiles/bruce-kim

2.5.2 Proposed TOF R&D Activities

We do not request FY19 R&D funds for the high-resolution TOF.

3. Lepton (electron) Identification

Contacts: C. Hyde <chyde@odu.edu>

The focus of the funded activities of the eRD14 Consortium is on hadron-species identification. However, we have not neglected electron and muon identification. At an Electron-Ion Collider, detection and identification of the scattered electron is a critical requirement. Also, many important processes involve particle decays to leptons (*e.g.*, $J/\psi \rightarrow e^+e^-$). The baseline system for e/π identification is the electromagnetic calorimeter (EMcal), which is included with 4π coverage in all the EIC model detectors. However, the pion suppression achievable in EMcal is limited primarily from charge-exchange events ($\pi^- p$ to $\pi^0 n$), resulting in an electromagnetic shower indistinguishable from an electron and associated with a charged track. Although different types of EM calorimeters have been considered for different parts of the EIC detectors, in general a good EMcal will provide e/π identification up to about 1:100. This can be improved with shape analysis of a high-granularity EM calorimeter, but at the cost of a loss of electron efficiency. Figure 3.1 illustrates the trade-off between PID detection efficiency *vs.* purity of PID, for a fixed PID separation of two species by $N\sigma$. The inclusion of a hadronic calorimeter (HCal) behind the EMcal will only partially improve the e/π identification, since charged pion events that charge-exchange in the EMcal will be mostly contained in the EMcal, and will not give large signals in the HCal. In order to reach kinematics where pion backgrounds are high, additional e/π ID detectors will be needed.

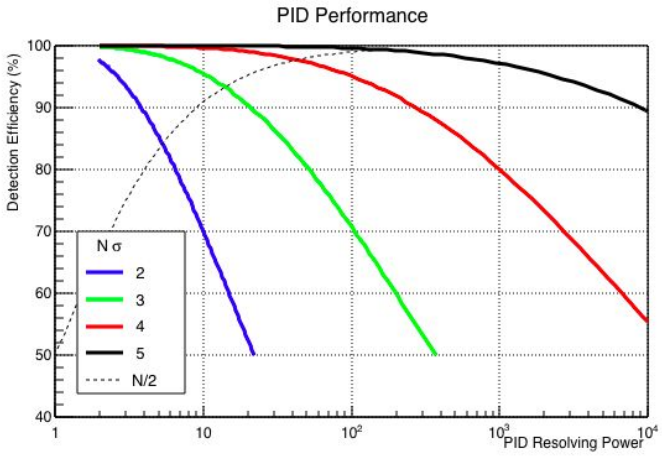


Figure 3.1: Contours of constant PID separation, $N\sigma$, in the plane of PID efficiency *vs.* resolving power *vis-a-vis* the unwanted species. The dashed line corresponds to making the PID separation at the midpoint between the two particle-species distributions.

3.1 Electron ID

In the hadron endcap, Fig. 2.1.5 demonstrates ≥3σ e/π separation up to 19 GeV/*c* by the proposed dual-RICH. For the C_2F_6 gas alone, ≥3σ e/π separation is achieved over the range 5–19 GeV/*c*. Thus, in the ion endcap, with the dual-RICH together with the EMCal, 10^3:1 e/π separation is achievable at ~95% electron efficiency up to 19 GeV.

On the electron endcap side, Fig. 3.2 (left) shows the large background from low-momentum pions. The mRICH (see section 2.3), if implemented in the electron endcap, will provide additional (to the EMcal) e/π discrimination, especially at low momentum, as illustrated in Fig. 3.2 (right). Following the dashed line of Fig 3.1, the combination of EMcal and mRICH can ensure less than 1% pion contamination in the electron sample over the entire momentum range of Fig. 3.2 (left). We have also proposed (although we do not request funds for FY18) the development of an e/π Cherenkov detector for the electron endcap – a common solution in electron scattering experiments (including CLAS12, SoLID, *etc.*). The technology we would like to pursue for the R&D is a variation of the Hadron Blind Detector (HBD) used at PHENIX, but with the sensors at the endcaps of the cylinder rather than around the barrel.

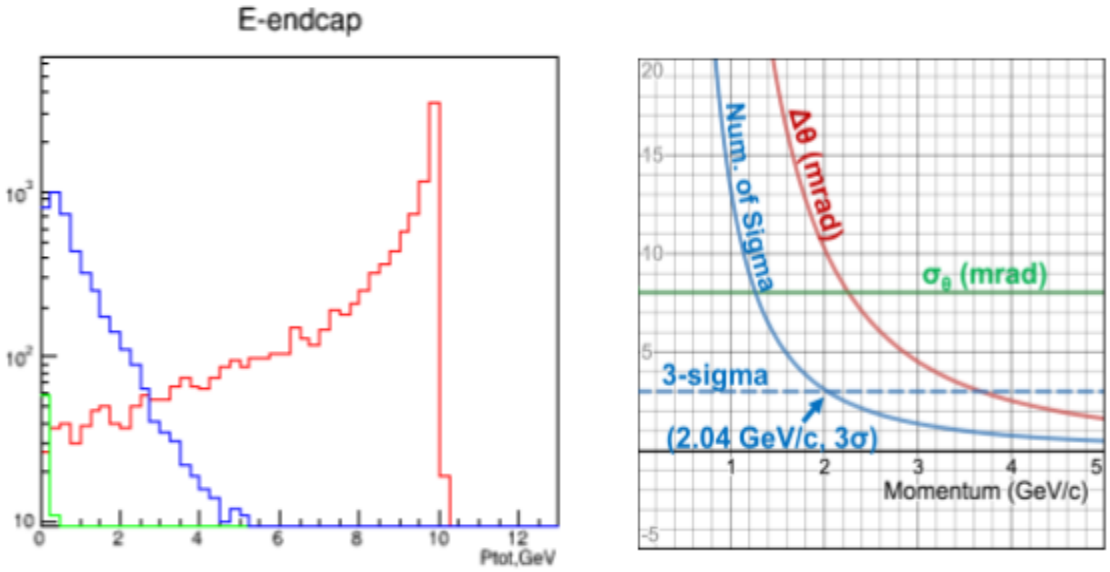


Figure 3.2 **Left:** Electron-endcap momentum distributions of scattered electrons (red), negative pions (blue), and secondaries (green) for collisions of 10 GeV electrons on 100 GeV protons (a common BNL / JLab kinematic) from Pythia in a bin of $1 < Q^2 < 10$ GeV^2 for the electrons (pions include photoproduction). **Right:** e/π discrimination beam-test performance achieved with the mRICH (section 2.3). The green line is the per-photon resolution (mrad). The red line is the e–π separation (mrad). The blue line is the achieved separation in experimental σ of the Cherenkov radii.

Figure 3.3, similar to Fig. 3.2, shows the particle multiplicities in the negative pseudo-rapidity side (electron-endcap side) of the central barrel region. Below 2 GeV/c, e/π discrimination is again challenging. Figure 3.4 outlines the e/π separation achievable with the DIRC. At 2 GeV/c, multiple scattering in the DIRC itself limits the tracking resolution to 1.5 mrad, and this degrades to 2.5 mrad at 1.3 GeV/c. The DIRC will still provide 5:1 e/π resolving power over this momentum range, with electron efficiency > 85%. This will provide an electron sample with less than 1% pion contamination for all momenta above ~1.3 GeV/c.

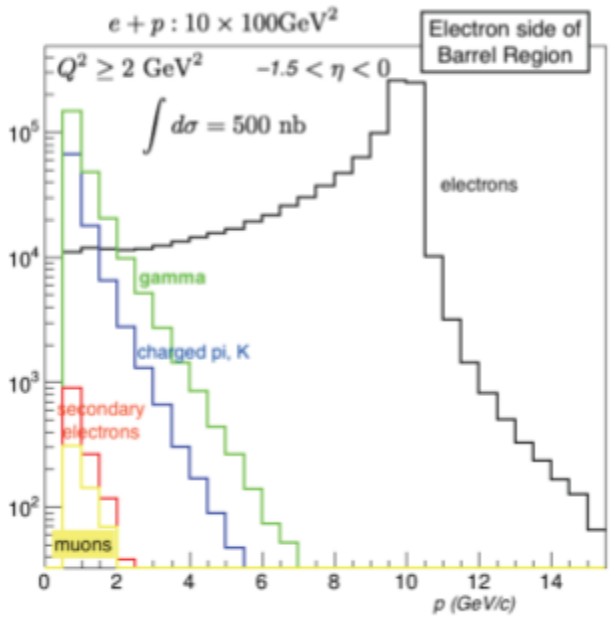


Figure 3.3: Central barrel region, negative-pseudorapidity (electron endcap side): momentum distributions of scattered electrons (black), photons from hadron decays (green), charged π/K (blue), electrons from hadron decays (red), and muons (yellow). The particles are produced in DIS of 10 GeV electrons colliding with 100 GeV/c protons. The events are selected for $Q^2 \geq 2$ GeV^2.

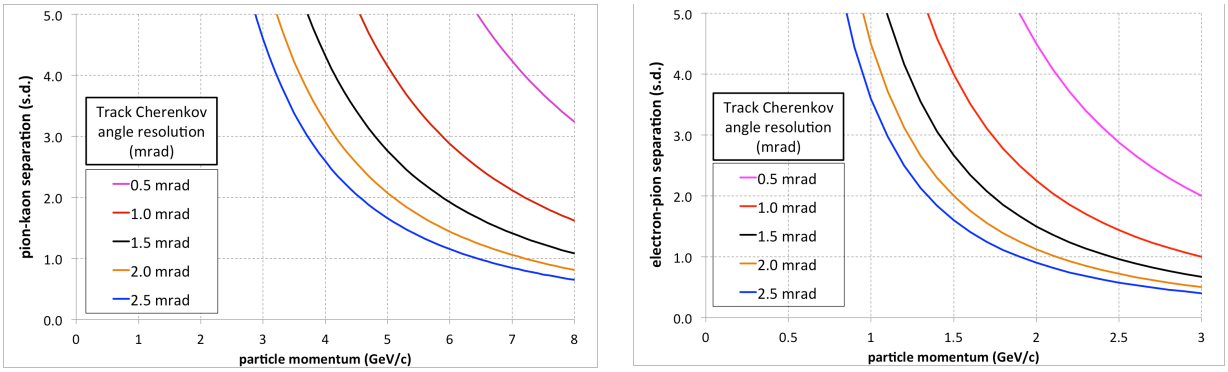


Figure 3.4: π/K separation (left) and e/π separation (right) in the DIRC in units of standard deviations (s.d.) as function of particle momentum for different values of the track Cherenkov angle resolution σ_c^{track}. A track Cherenkov angle resolution of 1 mrad is required to achieve 3 s.d. π/K separation at 6 GeV/c and 3 s.d. e/π separation at 1.7 GeV/c.

3.2 Muon ID

Muon identification is important for di-lepton production (both inclusive and vector meson decays, *e.g.*, J/ψ) and for semi-leptonic decays of heavy-flavor hadrons. Every EIC detector concept includes some form of hadron calorimetry in the ion downstream endcap of the central detector. However, the different proposals differ significantly in the central barrel region. We are assessing the Belle (and its Belle-II upgrade) K_{Long} – Muon (KLM) detector as a modest-cost option for instrumenting the solenoid return yoke. This has shown good performance for muon ID and modest performance for measuring the energy of high-energy neutrons and K-long mesons.

4. Photosensors & Electronics

The specific requirements that the DIRC and the RICH detectors must fulfill within the scope of the EIC pose unique constraints on sensor and electronics performance different from any previous DIRC and/or RICH implementation. Table 1 below lists the minimum requirements on DIRC, mRICH, and dRICH photosensors. Specifically, the small pixel size of 2–3 mm and the immunity to magnetic fields of magnitude in the range 1.5–3 T are unique constraints. The main objective of this R&D effort during the proposed funding period is to identify and assess suitable photosensor and electronics solutions for the readout of the EIC Cherenkov detectors, both for the full EIC detector and for prototypes in beam tests. Depending on the evaluation outcome, design optimization studies of those photosensor and electronics parameters that are found lacking in the evaluated samples but critical for operations in the EIC environment, will be carried out. In addition to supporting the adaptation of developing photo-sensor technologies for the EIC Cherenkov detectors (such as LAPPDs and GEMs) the goal is to identify a cost-efficient common readout solution that is shared within the EIC-PID consortium. Ultimately, in the long term, this R&D work will allow us to make a recommendation about the best photo-sensors and electronics solutions for the PID detectors in EIC implementation.

Sensor requirements and options

The consideration of possible photosensor solutions for each detector component is driven by the operational parameters of the detector, with cost optimization in mind. The table 4.1 below summarizes the performance parameters that photosensors for the DIRC, mRICH, and dRICH must satisfy.

Parameter	DIRC	mRICH, dRICH
Gain	~10^6	~10^6
Timing Resolution	≤ 100 ps	≤ 800 ps
Pixel Size	2–3 mm	≤ 3 mm
Dark Noise	≤ 1kHz/cm^2	≤ 5MHz/cm^2
Radiation Hardness	Yes[6]	Yes[6]
Single-photon mode operation?	Yes	Yes
Magnetic-field immunity?	Yes (1.5–3 T)	Yes (1.5–3 T)
Photon Detection Efficiency	≥ 20%	≥ 20%

Table 4.1 A list of performance requirements for the photosensors for the EIC PID Cherenkov detectors.

[6] The EIC radiation levels can be inferred from current operations at RHIC, and will depend on the sensor location.

The key parameters of the photodetectors for the mRICH are small pixel size, resistance to magnetic field, and low cost (due to its large sensor area). Depending on the mRICH location, the requirement for radiation hardness will vary. The detector does not require good PMT timing resolution. GEMs with a photocathode sensitive to visible light, with their good radiation hardness and good position resolution, would be a very good and cost-effective solution for the mRICH. SiPMs could be used where their radiation hardness is sufficient. MCP-PMTs such as LAPPDs with pixelated readout could be considered as possible photosensors for mRICH detectors if they have sufficient resistance to magnetic fields. In the final EIC detector, it is possible to use different photosonsors in different locations (LAPPDs could, for instance, be use near the beam where the radiation is high and SiPMs away from the beam, where the angle of the magnetic field changes more rapidly).
The key parameter of the photodetectors for the dRICH is the small pixel size. Although the relative sensor area (normalized to the absolute detector area) of this detector is small, due to the large absolute detector area, cost is also an important parameter. Good sensor options for the dRICH would be similar to the ones for mRICH (keeping in mind that due to the location of the sensors, the requirement for radiation hardness is not as important for the dRICH).
The key parameters of the photodetectors for a DIRC are fast timing, small pixel size, and a moderate to low dark count rate (DCR). Magnetic-field tolerance is required if the DIRC readout is located within the magnetic field of the solenoid. SiPMs might be possible to use for a DIRC if future developments lower their DCR to an acceptable level. Currently, the only photodetectors satisfying these requirements are MCP-PMTs (including LAPPDs with pixelated readout). Excellent timing resolution (~100 ps RMS) is in particular required for the high-performance DIRC if a time-based PID reconstruction method is adopted for the geometry based on wide radiator plates. Such timing resolution is satisfied by currently commercially available MCP-PMTs, however, development of electronics with good time resolution for small signals may be required.

4.1 Sensors in High-B fields

Contacts: Y. Ilieva <jordanka@physics.sc.edu>, C. Zorn <zorn@jlab.org>

The integration of the three Cherenkov detectors in the central detector involves setting their photo-sensor readouts in the non-uniform fringe field of the solenoid. While an out-of-field readout option for the DIRC may be feasible, an in-field readout is the only option for the two RICH detectors. The objective of this activity, thus, has been to assess the gain and the timing performance of available photosensors in high magnetic fields (due to the maximum field of 5 T attainable by the magnet, we can do the assessment from 0 T up to the field magnitude at which the sensor performance breaks down) and for various relative orientations between the sensor and the magnetic field, and to reasonably support (as needed for the R&D) further design optimization studies of these sensors. The long-term goal of the research is to recommend sensor options for Cherenkov-detectors readout in the magnetic field of the solenoid magnet.

4.1.1 FY18 Progress and Achievements

The program for testing photosensors in high magnetic fields was established within eRD4, and has now

been taking data for a sixth year. In the past two years, the main focus of the activities was the gain evaluation of a multi-anode Planacon MCP PMT with a pore size of 10 μm. The initial gain studies of single-anode MCP-PMTs with pore size of 3-μm and 6-μm yielded a reasonable performance up to 2 T (although that upper limit depended on the sensor, the applied high voltage, and the orientation of the sensor relative to the field) and showed that overall, sensors with smaller pore size can be operated up to higher magnetic fields. Large gain variations (of about an order of magnitude), depending on the sensor type, with (B, θ, φ)[7] were also observed. Since the readout of the EIC Cherenkov detectors is considered to be in an area where the solenoid field is non-uniform, finding a way to recover the gain not only at large B, but also for a large range of relative orientations between the sensor and the B-field is critical. Our gain studies, varying independently the voltages across the three stages: between the photocathode and the MCP ($V_{C\text{-}MCP}$), across the two microchannel plates ($V_{MCP\text{-}MCP}$), and between the last MCP and the anode ($V_{MCP\text{-}A}$), showed that optimizing the voltage across the multi-channel plates can help to recover the gain in B-fields. However, the range of B-field magnitude over which the gain can be fully recovered strongly depends on the angle between the sensor and the field axes. This means that high-voltage optimization alone cannot achieve gain recovery and uniformity over a large range of sensor-field orientations in a field of 3 T.

The results of the single-anode sensor measurements showed that (a) the best multi-anode MCP-PMTs candidates for EIC application are the ones with the smallest pore size and (b) gain measurements varying independently the voltages across the three MCP-PMT stages are important in order to identify the limits of gain optimization and uniformity over a large range of sensor-field orientations by controlling the HV, which is an easily accessible operational parameter.

Currently, the smallest pore size of commercially available multi-anode MCP PMTs is 10 μm and there are two manufacturers that have been producing such sensors, Hamamatsu and Photonis. Photek is in process of developing a small-pore-size multi-anode sensor, which could be of interest for EIC when it becomes available.

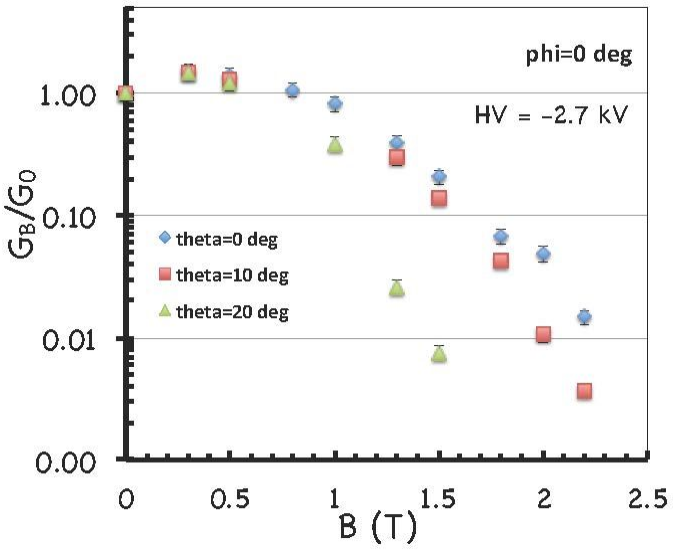


Figure 4.1.1: Relative gain of ch. 35 of 10-μm pore-size Planacon MCP PMT as a function of magnetic-field magnitude. θ is the angle between the normal to the PMT's front and the B-field vector. Above fields of 1.3 T the gain at θ=10° decreases faster with B than at 0°. Above fields of 1 T, the gain at θ=20° decreases faster with B than at 0° and at 10°. This narrows the maximum field at which the sensor can be operated at these orientations. The error bars show preliminary 14% uncertainties dominated by systematics.

[7] Here θ is the angle between the sensor and the B-field axes and φ is the rotation angle about the sensor axis.

In the Summer of 2017 the gain of Planacon (10-μm pore size) multi-anode MCP PMT was measured as a function of B and $\theta = 0^{\circ}$, 10°, and 20°. The results are shown in Fig. 4.1.1. The data were obtained by illuminating only two detector channels. The gain increases at small field magnitudes and reaches a maximum at 0.3 T for all test orientations. Above 0.3 T the gain decreases as the B-field increases, however the rate of decrease increases as θ increases. The high voltage on the PMT at which the tests were done was 96% of the maximum recommended value.

The gain of the 10-μm Planacon was also measured as a function of B and θ for $\varphi = 0^{\circ}$, 90°, 180°, and 270°. The gain variation over φ is much weaker than the variations over θ and B.

Since the pulse-height spectra of this Planacon PMT have the single-photoelectron peak well separated from the pedestal up to B-field of 1 T, we could estimate not only the PMT gain from fits to these spectra, but also obtain the average number of photoelectrons, μ, for each setting (B, θ, $\varphi = 0^{\circ}$). These results are shown on Fig. 4.1.2 and show interesting features. While at $\theta = 0^{\circ}$, both the gain and the number of photoelectrons increase as the field increases to 0.3 – 0.5 T and decrease at larger B, at the larger θ angles, the number of photoelectrons decreases steadily as the field increases and does not show a maximum at ~0.3 T as the gain. These trends suggest that at these larger θ angles not all photoelectrons emitted from the photocathode create an avalanche in the microchannel-plates. One hypothesis that could explain this effect is that the transverse B-field at these angles is sufficiently large so that the radius of curvature of the trajectory of some photoelectrons is too small for the photoelectrons to reach the first MCP. The data show that the larger θ is, the larger the loss is: about 25% at 10° and about 50% at 20°, which is qualitative consistent with the hypothesis. Simple calculations can be done, once the distance between the photocathode and the first PMT is known, to check if this explanation is reasonable. Above 0.3 T the loss of photoelectrons does not depend strongly on the B-field magnitude. To decrease the loss, one can increase the speed of the photoelectrons by increasing the voltage between the photocathode and the first MCP. This will be experimentally tested in Summer 2018.

Our 2017 gain evaluation results show that the B-field, combined with the sensor orientation, affects not only the gain, but also the efficiency of the MCP-PMT and that both quantities need to be monitored in the assessment of MCP-PMT performance in high magnetic fields. The accurate extraction of both parameters, depends strongly on the quality of the MCP PMT, as it relies on fits to pulse-height distributions in which the single-photoelectron peak is well separated from the pedestal. During the rest of FY18, we will study alternative methods for simultaneous determination of G and μ, which could be applied to our previous measurements of other MCP PMTs where the fits could not be done over a broad range of B and θ.

In FY18 we acquired and built the infrastructure needed for PMT time-resolution studies. A custom laser box for our pico-second laser has been manufactured and equipped with a safety interlock, which turns the laser off if the box is accidentally opened during measurements. This box could be adapted to hold a different laser should the need arise to acquire a faster laser. A 35ps resolution TDC was acquired on loan and implemented in our Data Acquisition System. During the rest of FY18, we will commission the timing branch of the setup and, if time allows, will perform first time-resolution measurements of a 10-μm Planacon MCP PMT.

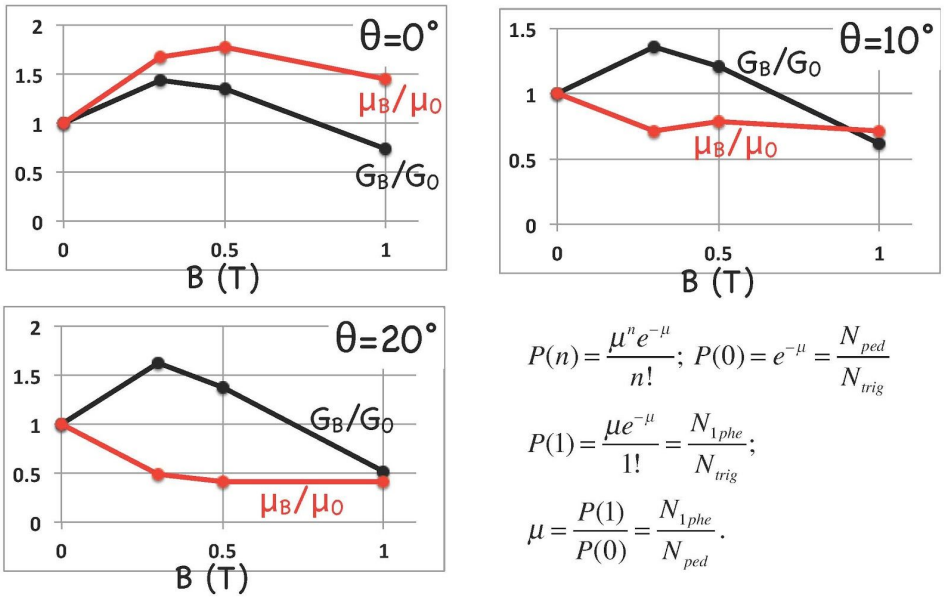


Figure 4.1.2: Red: Average number of photoelectrons (normalized to the number of pedestal events), μ, as a function of B-field and angle θ. **Black:** Gain, G, as a function of B-field and angle θ. Both G and μ are reported in units of the corresponding values at 0 T. In the equations in the bottom right, $P(n)$ denotes the probability to observe n photoelectrons.

In the Summer of 2018 we will

- study the gain of a 10-μm Planacon for various B-fields as a function of the high voltage between the photocathode and the first MCP, between the two MCPs, and if time permits, between the last MCP and the anode. The goal of this study is to identify the extent to which the gain and efficiency can be recovered by varying separately the high voltages across the three stages, and especially between the photocathode and the first MCP.
- study the amount of ion feedback for various magnetic fields and high voltages, as recommended by the review committee in January 2018. This will be done by assessing the relative number of after-pulses (normalized to the number of main pulses) arriving in a time range of ~10 ns to 500 ns after the main pulse; the evaluation will be done for varying high voltage at a constant B and for varying B at a constant high voltage in order to assess the driving cause of the feedback.
- commission a pico-second laser as well as timing electronics for time-resolution studies and take first time measurements with a 10-μm Planacon.

4.1.2 Proposed High-B R&D Activities

The main focus for FY19 is to perform a detailed time-resolution evaluation of a 10-μm multi-anode Planacon in magnetic fields from 0 T up to the maximum field where the gain measurements show that the PMT performance breaks down. The requested budget in the 60% and 80% scenario includes the cost of the cryogens required to cool the magnet and operate it over 2 weeks of measurements, of small components, such as boards, holders, connectors, *etc*. needed to readout the sensor and operate it in the dark box, and of travel of USC personnel (one faculty and two students) needed to prepare for and

perform the measurements. The 100% budget includes salary support for a second USC undergraduate student and for a high-resolution TDC. A second undergraduate student working on the project will provide needed manpower to maintain longer shifts, take and analyse more data and overall to yield a larger output of the FY19 activities. The need for more USC personnel is due to colleagues relocating for new appointments and not being able to take shifts and perform data monitoring and analysis during the measurements with a cold magnet. Purchasing a TDC mitigates the risk of not being able to borrow a TDC from another group for the FY19 measurements. The motivation for the timing-resolution measurements is given below.

Given the large gain variations with (B, θ, φ) observed in our measurements during FY14–16, and the solenoid field non-uniformity in the area where the installation of the DIRC[8] readout is considered, it is clear that the gain across the readout will not be uniform. Since the timing resolution of an MCP-PMT depends strongly on the amplitude of the output signal, *i.e.* the sensor's gain, the evolution of the sensors timing response with (B, θ, φ, HV) needs to be considered. A theoretical model of the electron avalanche development in the MCP suggests that the transit time spread (TTS) of a straight-channel MCP should not depend on the component of the field parallel to the channel axis[9]. No theoretical input exists regarding the effect of transverse fields. Actual timing measurements of chevron-stacked MCPs exist only for magnetic fields up to 2 T. The study done for the development of the BELLE II TOP counter evaluated the timing resolution of a multi-anode Hamamatsu sensor up to 1.5 T for a fixed orientation of the sensor axis relative to the field and found no significant changes[10]. A more comprehensive study was done for the development of the PANDA DIRC as the timing performance was evaluated not only for varying fields but also for varying orientations between the sensor and the field axes[11]. Within the uncertainties of their measurements, the letter study found only a small deterioration of the time resolution towards higher fields. As this study covered a range of fields up to 2 T only, there are no data mapping MCP-PMT timing response above 2 T and it is not known if the observed small deterioration would follow a progressive trend at higher fields. While, based on the published low-field measurements, one expects the timing resolution to deteriorate (if indeed) as the field increases much less than the gain, given the requirement of 100 ps or better timing resolution for the EIC DIRC, it becomes important to evaluate MCP-PMT timing characteristics with (B, θ, φ, HV). Naturally, timing measurements will strongly relate to the gain measurements and will also follow up with sensor design optimization as well as with advancements in performance of timing readout electronics. Extending the functionality of the High-B test setup to allow for precise timing measurements is also a natural synergistic activity with the LAPPD project.

Our goal for the future effort of the High-B program is to achieve an MCP-PMT design and operational parameters that are optimized for successful application in the Cherenkov PID detectors in the high magnetic field of the central detector at EIC. This effort will involve (a) High-B timing studies of a variety of commercially available multi-anode MCP-PMTs as a function of various operational parameters, (b) Development and implementation of a simulation of an MCP-PMT in the design process.

[8] DIRC is explicitly mentioned here, since excellent timing resolution is key for the DIRC time-based PID method..
[9] G.W. Fraser, Nucl. Instr.. Meth. **A 291**, 595 (1990).
[10] S. Hirose, Nucl. Instr. Meth. **A 766**, 163 (2014).
[11] A. Lehmann *et al.*, Nucl. Instr. Meth. **A 595**, 173 (2008).

Proposed R&D Activities

FY19

- Evaluation of the timing resolution of a multi-anode 10-μm pore-size Planacon as a function of (B, θ, φ, HV).
- Work on development of MCP-PMT simulation as time permits.

FY20

- If available, evaluation of the timing resolution of a multi-anode 10-μm pore-size Photek sensor as a function of (B, θ, φ, HV).
- Shift the focus of effort on MCP-PMT simulations.

The proposed activities of the program are based on our results from the first six program years. As our efforts continue to develop, we will continue to benefit from the expertise of our PANDA GSI collaborators and from the established collaborations with MCP-PMT manufacturers, such as Photek, Photonis, and Hamamatsu as we proceed with the evaluation of their sensors.

4.1.3 High-B R&D Deliverables

FY19

- Report on multi-anode PMT (Planacon) timing resolution as a function of (B, θ, φ, HV).
- Progress report on MCP-PMT simulation studies.
- Publication of our 2014 – 2018 results.

4.2 LAPPD™ MCP-PMTs

Contacts: J. Xie <jxie@anl.gov>, M. Chiu <chiu@bnl.gov>

The LAPPD™ project is a multi-year project involving a number of institutions, with a goal to create an MCP-PMT that has the same very high performance as existing MCP-PMTs, but at a significantly lower cost. Specifically, for the EIC detector R&D, the effort aims to adapt the LAPPDs to the EIC requirements, which include pixelated readout and acceptable performance in high magnetic fields. With these adaptations, the LAPPDs can be used for the readout of mRICH, dRICH, and DIRC sub-systems as well as for TOF applications.

4.2.1 FY18 Progress and Achievements

The first magnetic-field tolerance performance test of a 6cm MCP-PMT was successfully performed at the Argonne g-2 magnetic-field facility. Experimental data obtained in the run were analyzed to establish the baseline of magnetic-field tolerance of the 6cm MCP-PMT with current standard LAPPD design. The dependence of the 6cm MCP-PMT response, in terms of the mean pulse height, on the magnetic field strength at different high voltages was compared for two types of 6cm MCP-PMTs with different designs (the result with an initial internal-resistor chain design was obtained in a previous JLab testing). The initial internal-resistor chain design relies on the resistances of ALD coated MCPs and spacers for high

voltage distribution. However, due to the irregular reduce of MCPs and spacers resistances during the baking and scrubbing process, it was impossible to achieve the designed HV distribution for optimized MCP operation. The newly developed, independently-biased design introduces HV connections for the MCP top and bottom surfaces individually, so that the HV on each MCP can be optimized independently. The test results show that the initial internal-resistor chain design only achieves magnetic-field tolerance up to 0.15 T (see Fig. 4.2.1(a)), while the independently-biased design achieves magnetic field tolerance up to 0.7 T (see Fig. 4.2.1(b)) with both MCPs operating at a proper HV. The angular dependence of the MCP-PMT response was additionally studied by rotating the MCP-PMT at angle θ relative to the magnetic-field direction, as shown in Figure 4.2.1(c). The results displayed in Figure 4.2.1(d) show the effect of the 8° bias angle of the MCPs, resulting in two performance maxima at θ ~ ±8°. The different intensities of these two peaks are due to the different effect from the top and the bottom MCPs.

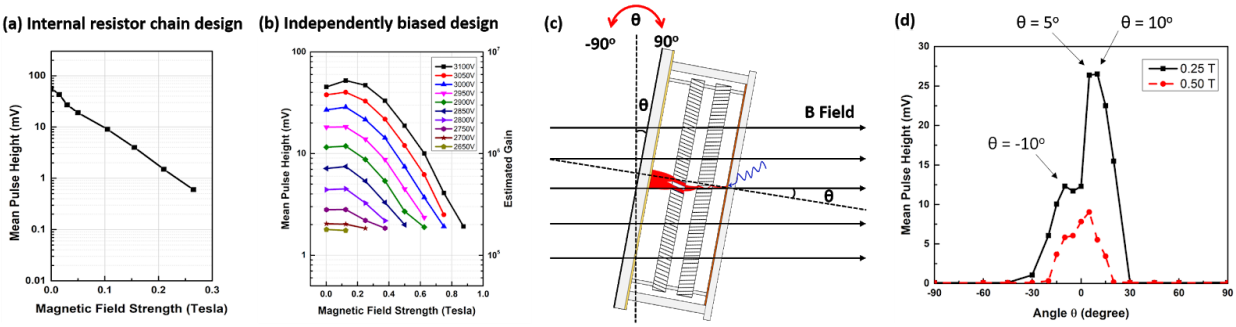


Figure 4.2.1: (a-b) Dependence of the 6cm MCP-PMT response, in terms of the mean pulse height, on the magnetic field strength at different high voltages: (a) Initial internal-resistor chain design: B field tolerance < 0.15 T, (b) Independently-biased design: B field tolerance < 0.7 T. (c) Schematic of the rotation mechanism of the MCP-PMT showing the rotation angle θ between the normal to the MCP-PMT front and the magnetic-field direction. (d) Response of the MCP-PMT as a function of the rotation angle θ. The two peaks around -8° and 8° reflect the 8° bias angle of the MCPs. Note that the intensities of these two peaks are not the same due to the different effect from the top and the bottom MCPs.

With the above encouraging results of the magnetic-field tolerance measurement, the Argonne group together with Incom, Inc. submitted a proposal entitled ***Magnetic Field Tolerant Large Area Picosecond Photon Detectors for Particle Identifications*** **to the DOE Small Business Innovation Research (SBIR) Phase I program**. The proposal **was awarded funding at $150k level with support period of Apr. 9, 2018 – Jan. 9, 2019.** Since the award of the SBIR grant, Incom, Inc. has devoted a strong effort to develop low cost LAPPD^{TM} targeting EIC-PID applications.

In FY18, we also studied in detail parameters that affect the MCP-PMT magnetic field tolerance. We studied the dependence of the device performance on the applied high-voltage difference between the photocathode and the upper surface of the top MCP. Figure 4.2.2 (a) shows a schematic of the setup. The HV_{MCPs} was kept at a constant value, and the $HV_{Photocathode}$ was varied during the experiment. The results, plotted in Figure 4.2.2(b), show that there is an optimal HV difference yielding best performance. This finding can be explained by the MCP secondary-electron yield dependence on the primary electron energy, which has been studied in our previous work. An optimal primary electron energy, determined by

the HV between the photocathode and the MCP top surface, exists for best secondary electron emission as shown in Figure 4.2.2(c).

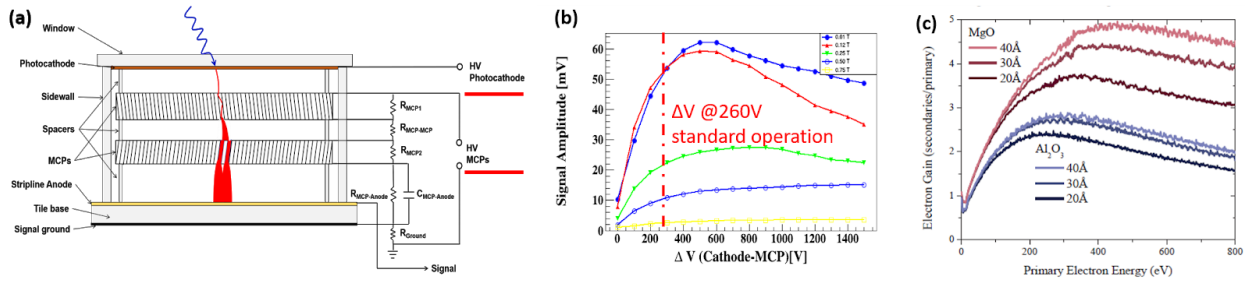


Figure 4.2.2: (a) Schematic of the experimental setup used in the study of the effect of HV; (b) Dependence of the 6cm MCP-PMT signal amplitude on the HV difference between the photocathode and the MCP top surface. The different curves have been obtained for different magnetic fields; (c) MCP secondary electron yield on dependence of primary electron energy (Ref: *S. Jokela et al. Physics Procedia 37 (2012) 740*).

Recently, Incom, Inc. delivered a functional 20 x 20 cm^2 LAPPD^{TM} to Argonne to establish a baseline of its magnetic-field tolerance. The 20 x 20 cm^2 LAPPD^{TM} was installed in the Argonne magnetic-field test facility (Fig. 4.2.3(a)), and the dependence of its performance on the magnetic-field strength, rotation angle, as well as biased high voltage was studied. Our preliminary results are consistent in magnitude and angular features with our earlier results for the 6cm MCP-PMT. Especially, we studied the LAPPD^{TM} performance dependence on the biased voltage at different gaps. The preliminary result indicates that bias voltages at all three gaps affect the gain of the LAPPD^{TM}. The bias voltage between the photocathode and the top MCP has the strongest effect. The LAPPD^{TM} gain becomes constant when the bias voltage between the bottom MCP and the Anode is above a certain threshold. The HV applied to the MCPs seems to have no preference as both, HV on MCP1 and HV on MCP2 equally affect the LAPPD gain. Detailed data are under analysis and will be reported later.

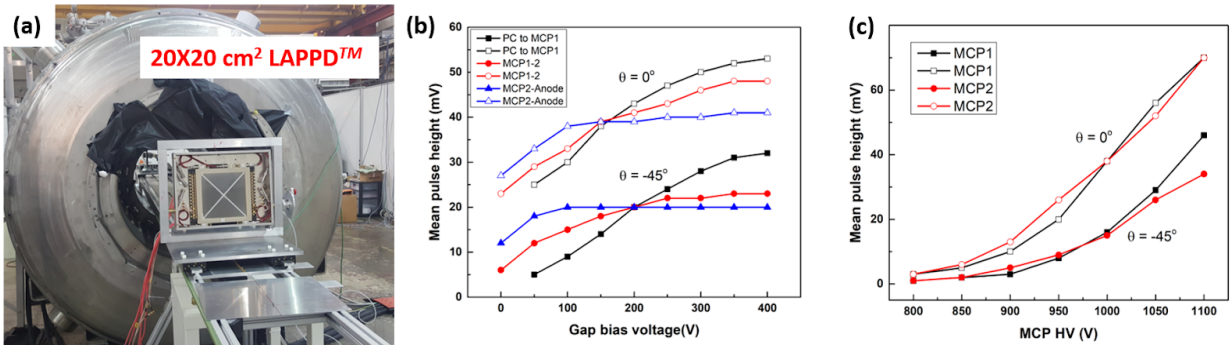


Figure 4.2.3: (a) The 20 x 20 cm^2 LAPPD^{TM} installed in the Argonne magnetic-field test facility; (b) LAPPD performance dependence on the bias voltage applied to each of the three gaps in the LAPPD configuration, the MCP on top, close to photocathode, is labeled as MCP1 while the MCP at the bottom is labeled as MCP2; (c) LAPPD performance dependence on the bias voltage applied to the two MCPs.

Besides the magnetic-field tolerance study of the 6cm and the 20cm LAPPDs, we also performed a beamline particle experiment on a demountable MCP-PMT with pixelated readout at the Fermilab test

beam facility. The Argonne MCP-PMT demountable chamber (Figure 4.2.4(b)) is designed to be a flexible setup to study the effect of different geometries on the MCP-PMT performance. The chamber is dynamically pumped with a turbo vacuum pump to maintain a vacuum of 10^{-7} torr. The chamber is held by an aluminum holder with a flat base to ensure stable placement on a flat surface. Inside the chamber is the demountable MCP and a signal-readout board. A very thin aluminum photocathode was coated on the top glass, following the top glass are two MCPs and a printed circuit board with different pad sizes. The whole stack is firmly compressed with set screws at four corners. The PCB board is pixelated with pad sizes of 2 mm x 2 mm, 3 mm x 3 mm, 4 mm x 4 mm and 5 mm x 5 mm (Figure 4.2.4(a)). The high voltages are provided to the MCPs via SHV vacuum feed throughs, and the signals are lead out via BNC vacuum feedthroughs. The high voltages are provided by a multichannel WIENER Mpod mini-crate, and the signal waveforms are collected by a CAEN DT5742B desktop digitizer. Figure 4.2.4(c) shows the demountable chamber installed on the platform of Fermilab's test beam facility.

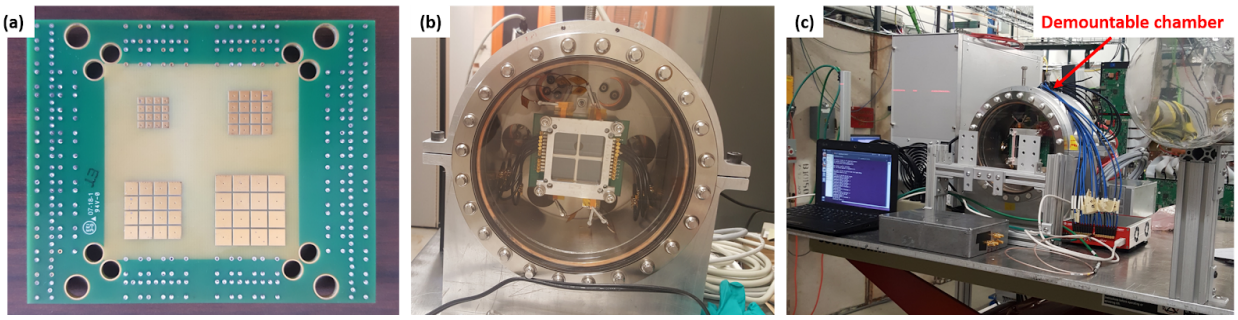


Figure 4.2.4: (a) A PCB board is pixelated with pad sizes of 2 mm x 2 mm, 3 mm x 3 mm, 4 mm x 4 mm and 5 mm x 5 mm. (b) An MCP-PMT stack with a pixelated readout board is installed in the Argonne demountable chamber. (c) The demountable chamber installed on the platform of Fermilab's test beam facility.

A 120-GeV proton beam was used to generate primary electrons in the MCPs, and the electrons were amplified and collected at the pixelized PCB board. Multi Wire Proportional Chambers (MWPC) with 1mm pitch were used as tracking stations, and correlated with the pad location (x-, y-axis). The spread of the difference between the pad location and the MWPC projection was fitted to obtain position resolution. Figure 4.2.5 shows an example of the correlation between the y-axis of a 3 mm x 3 mm pad and the MWPC projection, the spread fitting gives a position resolution of 0.93 mm. The position resolutions along x- and y-axis with different pad sizes are listed in Table 4.2.1 and show that the experiment results are close to the expected position resolution $\sigma(\text{expected}) = \text{pad size}/\sqrt{12}$.

Pad size	**2 mm x 2 mm**	**3 mm x 3 mm**	**4 mm x 4 mm**
σ (x)	-	1.01 mm	1.11 mm
σ (y)	0.73 mm	0.93 mm	1.43 mm
σ (expected)	0.6 mm	0.9 mm	1.2 mm

Table 4.2.1: Position resolution along x- and y-axis of the pixelated readout.

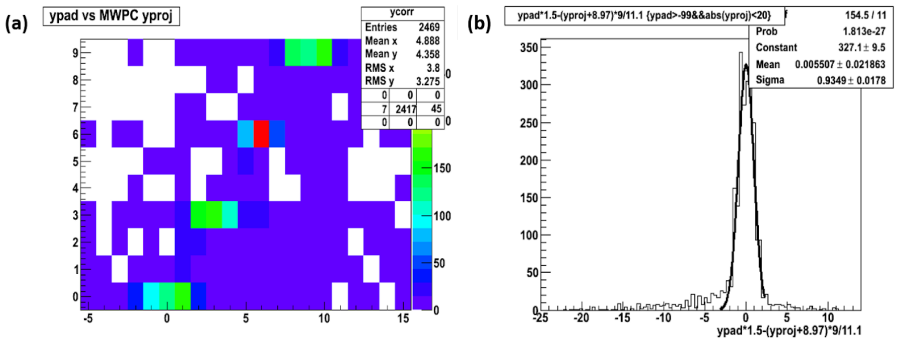


Figure 4.2.5: (a) Correlation between the y-axis of a 3 mm x 3 mm pad and the MWPC projection, (b) The fit of the spread of the position difference yields a position resolution of 0.93 mm.

With respect to the 6cm MCP-PMT/LAPPD production, four 6cm MCPs with 10μm pore size were received at Argonne from Incom, Inc. We are currently working to produce the first 6-cm MCP-PMT with a 10μm pore size and a reduced spacing this Summer. The device will be tested in the lab, including a magnetic-field measurement, in Aug. – Sep. 2018. MCPs with 5μm pore size, the smallest pore size of MCP that can be produced by Incom, Inc., were also ordered, and are scheduled to be delivered by the end of 2018.

4.2.2 Proposed LAPPD R&D Activities

FY19

- MCP-PMT afterpulse study to better understand the ion feedback for LAPPD.
- Improvement of RMS timing by modifying the bias voltages.
- Produce a detector with 5μm pore size MCP and minimum spacing to further improve magnetic-field performance and fast timing (possibly <10 ps) specifically for EIC applications.
- Test of MCP-PMT/LAPPD with different configurations (smaller pore size and reduced spacing) in lab and in a magnetic field.
- Demonstration of capacitive-coupling pixelated readout through ALD coated glass.

FY20

- Transfer the magnetic-field tolerant design to Incom, Inc. for 20cm LAPPD production.
- Testing of 20cm LAPPD with capacitive-coupling pixelated readout through ceramic base.
- Detailed testing of capacitive-coupling pixelated readout though ALD coated glass.
- Produce a 6cm MCP-PMT with capacitive-coupling pixelated readout through ALD glass.

4.2.3 LAPPD R&D Deliverables

FY19

- 6cm MCP-PMT with 5μm pore size MCP and minimum spacing.
- Demonstration of capacitive-coupling pixelated readout though ALD coated glass.
- Publication of a paper on the magnetic-field testing and capacitive coupling through glass.

FY20 (tentative)

- 20cm LAPPD with reduced spacing and small pore size MCPs.

- 6cm MCP-PMT with capacitive-coupling pixelated readout through ALD glass.
- Publication of papers on experimental results.

4.3 Readout Sensors and Electronics for Detector Prototypes

Contacts: G. Varner <varner@phys.hawaii.edu>, M. Contalbrigo <mcontalb@fe.infn.it>

The development of advanced, high-performance RICH and DIRC detectors poses new demands on photosensors and requires new readout electronics. All eRD14 Cherenkov systems envision using small pixels (2–3 mm), while the DIRC also needs to obtain good timing (< 100 ps RMS) with the relatively small pulses produced by MCP-PMTs. While initial prototype tests have been made with larger pixels and poorer timing to validate Monte Carlo simulations, which were then used to infer the performance of the systems developed for the EIC, future prototypes will have to be able to directly demonstrate the desired PID performance. To achieve this, new readout electronics has to be developed. In addition, while a demonstration of the PID performance can be achieved using simpler sensors (*e.g.*, MAPMTs for the two RICH detector prototypes), the final EIC application will impose additional constraints, such as operation in the magnetic field of the solenoid as well as a minimization of the total system cost. Thus, it is also important to be able to test alternative sensors, such as SiPMs for the RICH detectors.

To address the slightly different requirements and timelines of the various systems, we have developed a common consortium-wide strategy that provides a complete solution while maximizing synergies and minimizing cost. The Hawaii group will take the main responsibility for the development of the front-end electronics (ASICs and boards), while INFN together with JLab will have the lead on integration for both the sensors and back-end / DAQ. The development has been staged, from almost ready-to-go systems to provide a reliable reference based on a consolidated technology to innovative solutions optimized for the EIC prototypes. For the front end, the older MAROC-based system that was used in the first mRICH test beam (and is also used for CLAS12) has been adapted for sensors (MAPMTs, SiPMs) with smaller pixels. This will provide a fallback solution, and allow to explore different cooling options for the SiPMs. A new front-end is also being developed based on the waveform sampling TARGETX chip (first version ready for the 2018 mRICH beam test at Fermi Lab), which will be integrated on a board directly matching the footprint of the sensors. In contrast to MAROC, TARGETX can also provide the high-resolution timing required by high-performance DIRC detectors using time-based reconstruction algorithms. Ultimately, TARGETX would be replaced by the lower-power, higher-performance SiREAD chip. EIC experience with TARGEX would facilitate proper integration of the new chip. Nalu Scientific, LLC, a Hawaii based small business specializing in System-on-Chips for particle physics, in collaboration with the University of Hawaii has recently concluded a Phase I SBIR project to develop the SiREAD chip. The prototype 32 channel waveform sampling and digitizing SiREAD was fabricated and is currently under test. Figure 4.3.1 shows the fabricated SiREAD and the test setup together with preliminary SiPM readout signals.

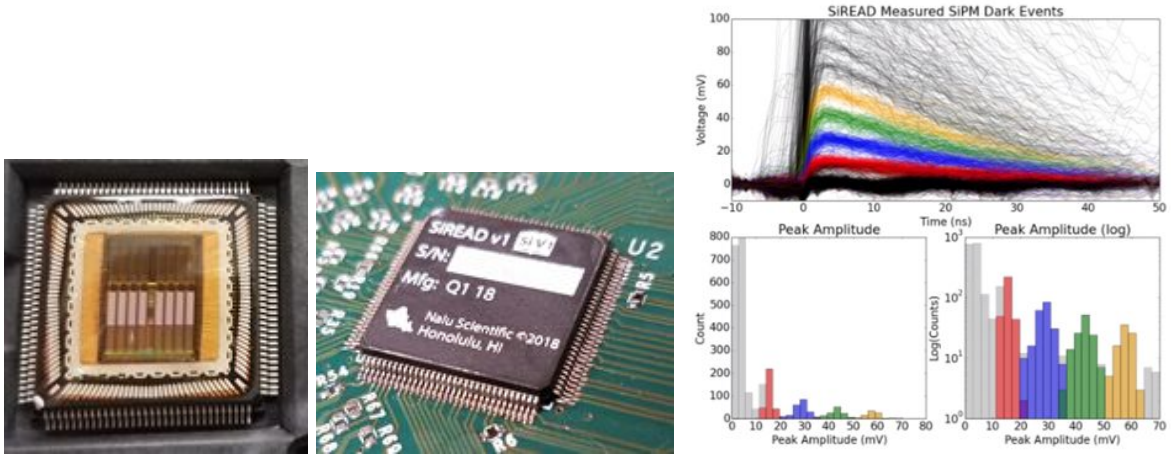


Figure 4.3.1: Micrograph of the fabricated prototype SiREAD (left). Prototype SiREAD on the evaluation PCB (middle). Superimposed dark count waveforms recorded from a SiPM using the SiREAD operating at 1 Gsa/s.

The SiREAD effort will also benefit from the ASoC (higher performance System-on-Chip), which has now received SBIR II funding. We hope that SiREAD will be available for instrumenting the PANDA DIRC prototype with small-pixel MCP-PMTs once the prototype is moved to the U.S. in FY19 specifically for the EIC R&D effort after the PANDA R&D is completed. For the back end we plan to use an adaptation of the data acquisition (DAQ) developed for CLAS12. The latter will be integrated with all three front ends and be able to collect data from multiple sensors. The new mRICH and dRICH prototypes, while allowing the performance study with more and more realistic optical components, will also serve as demonstrators during the development of the dedicated readout electronic, *i.e.*, TARGETX / SiREAD- based readout with common DAQ.

The use of sensors with a small pixel size (2–3 mm) should allow to validate the PID performance of the mRICH, dRICH, and high-performance DIRC prototypes. The H13700-03 MAPMTs acquired in FY17 by GSU provide the baseline solution for testing the optics of the RICH prototypes, a goal for which tolerance to magnetic fields is not required. SiPMs represent an innovative solution with several advantages potentially interesting for EIC (such as robustness, low bias voltage, cost-effective industrial production, magnetic-field compatibility, low material budget), but also some limitations (high noise, low radiation hardness). For the DIRC, MCP-PMTs with a similar footprint will be required to provide the desired timing performance. This is also the type of sensor that would be used in a final DIRC application.

4.3.1 FY18 Progress and Achievements

In FY18, a reliable readout system for the mRICH prototype has been realized by adapting the two front-end electronics based on the MAROC and TARGETX chips to sensors of small pixel size. The back-end, initially based on a generic TCP/IP protocol, has been migrated to the SSP protocol developed for the CLAS12 RICH DAQ. The new protocol offers a scalable solution compatible with the various front-end chips and has been already integrated with the MAROC chip. The development of a custom solution for SiPM matrices integrating a cooling system has been initiated.

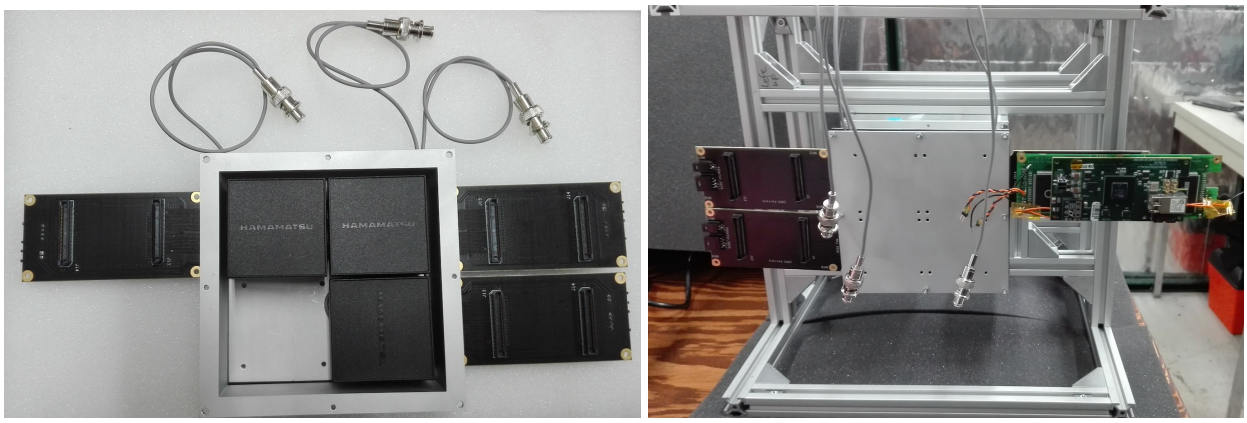


Figure 4.3.2: MAPMTs assembling for mRICH prototype. The adapter boards distribute the 256 channels of one Hamamatsu H13700 sensor over two 128 channel MAROC boards mounted on opposite side (front and back).

The electronics developed for CLAS12 has been designed to readout MAPMTs and to be compatible with SiPMs. In order to match it to the H13700 sensors, an adapter board distributing the 256 channels (16x16) over two MAROC readout units has been realized (see Fig. 4.3.2). In order to readout several units during the mRICH prototype test, a complete CLAS12 DAQ chain has been borrowed to be used with the JLab SSP protocol and a dedicated stand-alone acquisition software. Being designed to serve a complete detector, such a DAQ system is suitable for EIC, but represents an over-sophisticated and costly solution during a prototype phase. The INFN and JLab groups aim to realize a simplified version to be distributed among the consortium groups. The funding request covers the development of such a basic system and ensures the availability of a dedicated and flexible DAQ hardware over the extended EIC R&D time period. The large number of sensor's channels to be readout imposes a compact, modular, and fast data acquisition system (DAQ). In addition, DAQ needs to provide single channel timing information (~few hundreds ps resolution or better) and possibly charge information (the smaller gas rings show a simulated photon multiplicity on a single pixel of approx. 1.3). The Hawaii group is developing new front-end chips based on SiREAD, suitable for SiPM. The chip will be readout by a proper porting of the recent DAQ system developed for the CLAS12/RICH, and based on a powerful optical link between the generic programmable FPGA front-end board and the VSX sub-system processor back-end board. This synergy would speed up and simultaneously reduce development costs. In case the Hawaii front-end chip would not be available, the mentioned CLAS12/RICH DAQ could be temporarily adopted in conjunction with the original MAROC front-end chip for prototyping. The proposed back end and DAQ based on the SSP protocol will be compatible with both the current CLAS12 (Maroc-based) front end electronics, and the new (TARGETX, SiREAD) electronics developed by U. Hawaii.

The INFN groups have already experience in studying the performance of SiPM in the single-photon regime for Cherenkov applications. Promising results were obtained but additional work is needed to prove a realistic working condition in single-photon mode, taking into account the high dark count rate and the performance degradation resulting from irradiation. INFN has several SiPM matrices of various

sizes and, in particular, 3 large 16x16 MPPC matrices which are comparable with the H13700 pixel geometry, see Fig. 4.3.3. The large matrices are BGA mounting and should be mounted on a dedicated PCB supporting a cooling system for temperature control.

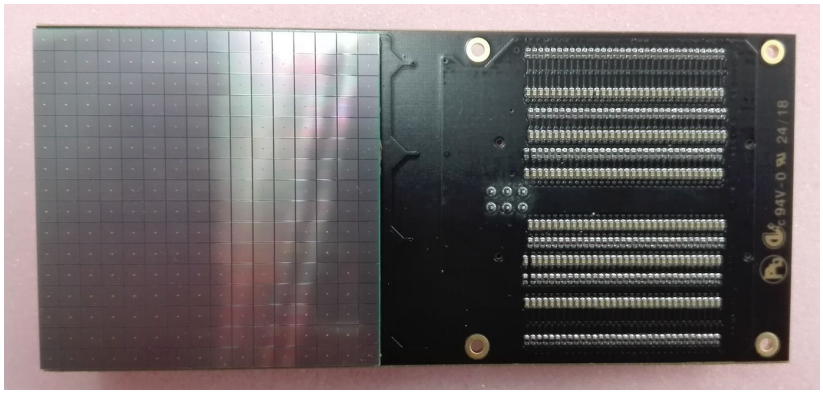


Figure 4.3.3: SiPM matrix mounted on a PCB integrating a cooling frame in the back plane.

Highly integrated, low-power, and high-performance readout of 256-anode, 50-mm photosensors is being studied at the University of Hawaii, which has extensive experience in developing electronics for modern PID systems, such as the Belle II TOP DIRC. The proposed system can be adapted to read out all the photosensors (MaPMT, MCP-PMT, SiPM) that are being considered for the various RICH and DIRC detector prototypes being developed by the EIC PID consortium. A compact board stack mates in the envelope directly behind the photosensors, permitting seamlessly abutting together an array of such devices. Each board stack consists of an interface board, which mates directly to the photodetector high-density signal connectors and hosts the waveform sampling ASICs, as well as a digital interface node. A simple and standard power and serial interface allows groups of these 256-anode devices to be collected into a single ethernet acquisition node. The first version of this readout will use a TARGET family ASIC, which has been successfully deployed in 10's of thousands of channel quantities for applications such as large muon systems or atmospheric gamma Cherenkov camera readout. Pairs of these 16-channel ASICs are mounted onto tiny DIMM cards, mounted onto the interface board. As a second phase, reduced power and further compactness will be realized by upgrading to the 64-channel SiREAD ASIC, when it becomes available. Both the TARGET and SiREAD ASICs are developed by the Hawaii group (TARGET at University of Hawaii, and SiREAD as a commercial product at Nalu Scientific). The high-speed sampling used by both chips provides the timing resolution required for the DIRC and can provide readout of waveforms during test beam conditions, which can be helpful for interpreting the data. Funding is requested for $20k of a graduate student time to complete the layout of the 3 boards, coordinate their assembly, verify functionality of first prototypes, and characterize their performance. The cost of the fabrication and population of these first prototypes is estimated as $10k, including printed circuit board and component costs.

In the first year of the Readout Sensors and Electronics for Prototyping activities, the goal was to instrument a 4 PMT modular RICH prototype. The PMTs are challenging in that these 2” PMTs have a

rather dense anode array of 256 signal channels each. As a first stage, the readout makes use of the existing TARGETX family of 16-channel transient waveform digitizing ASICs. This compact solution benefits from integrating all trigger, sampling and analog-digital conversion functionality in the same ASIC. Therefore a relatively compact 4x4 array of these chips is able to instrument each PMT. To further speed development, a standard control and readout programmable logic unit, the SCROD, which was developed for the Belle II muon system upgrade has been adopted. While this reduced significant the initial prototyping costs, the form factor is not compatible with a final, tiled-array of readout photosensors. All the requisite boards have been fabricated and will be tested in the Fermilab test beam facility. The complete system diagram is shown in Fig. 4.3.4.

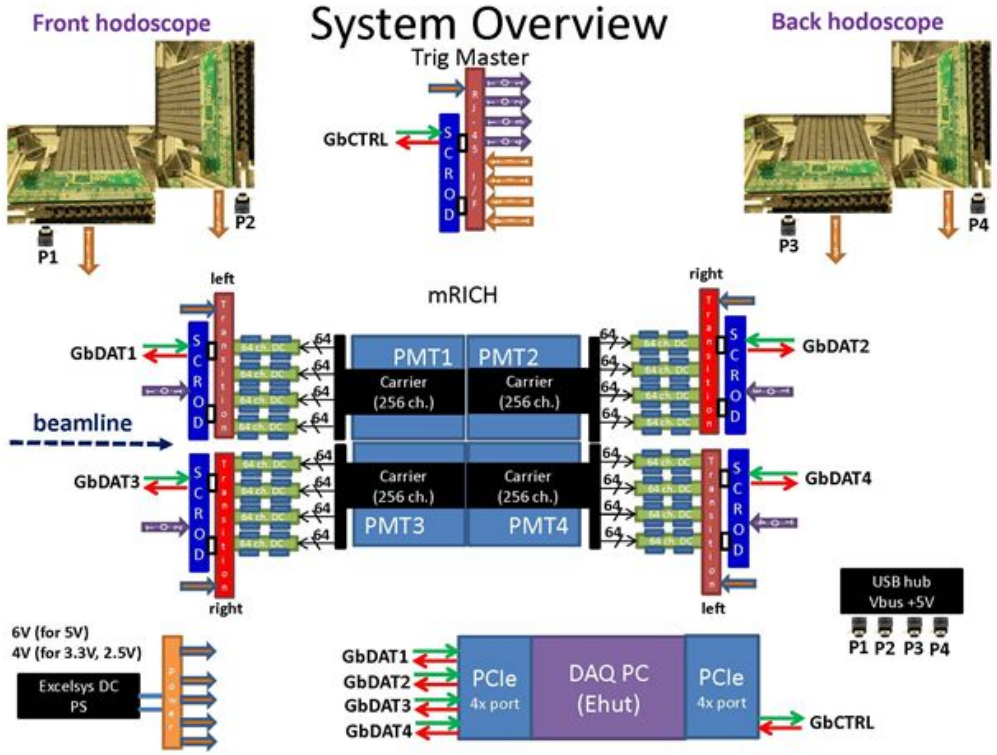


Figure 4.3.4: Overview of the 1k channel modular RICH prototype readout, which is built upon the TARGET ASIC and SCROD control and readout module.

A photograph of the first PMT assembly is shown in Fig. 4.3.5. In order for these 4 PMTs to abutt, the design has them arrayed in a 'pinwheel' configuration, as shown in Fig. 4.3.6. This is something that will be addressed by the higher integration density of the future SiREAD ASIC and next-generation FPGA board.

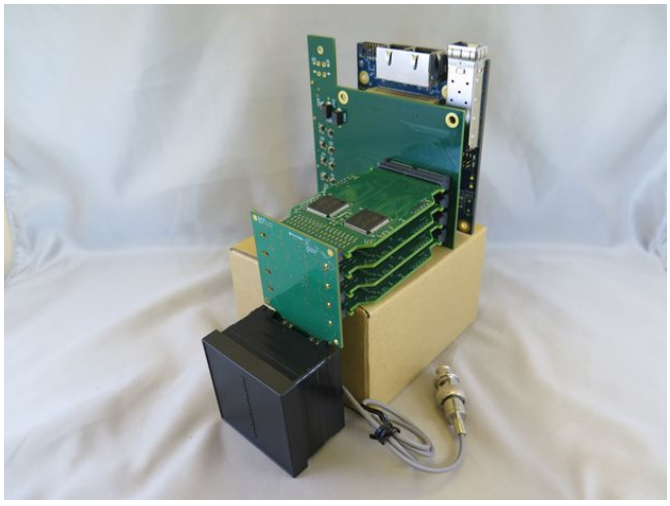


Figure 4.3.5: Photograph of the first generation of 256-anode 2" PMT readout for use in the Fermilab beam test facility.

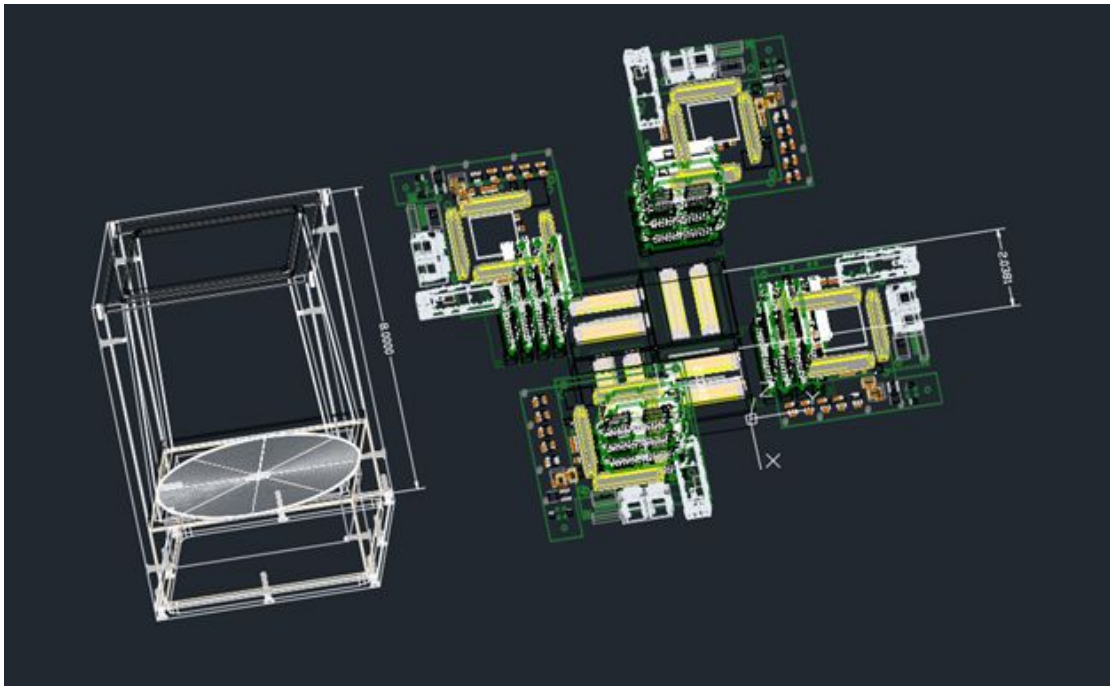


Figure 4.3.6: Prototype readout configuration, where a 'pinwheel' configuration has been used to permit the 2x2 PMT array to be abutted. While the initial design had the readout directly behind the PMT, because the current SCROD form-factor could not fit in the envelope behind the PMT, it was decided to use a Carrier board, which would offset the TARGETX and other cards and permit a simpler mechanical support and light-sealing. Next generations of the readout will use increased integration density to permit a low-profile readout that will fit within the envelope behind the photosensor and allow indefinite tiling of photosensors and their readout.

To further reduce cost and further integration, compactness and reliability the next stage of development will implement the SiREAD ASIC. In addition to increasing channel density from 16 to 64 channels, most of the state-machine control infrastructure provided by the companion FPGA will be integrated as "system on chip" functionality. This significantly reduces the digital interconnection burden and will make the system more scalable and make better utilization of a reduced number of gigabit fiber optic links used for control and data acquisition.

Table 4.3.1: SiREAD specifications.

SiREAD Parameter	Specifications
Channels	64
Sampling rate	1-4 GSa/s
Storage samples/ch	4096
Analog bandwidth	0.7-1.1 GHz
RMS voltage noise	<1mV
Dynamic range	10-11 bits
Signal voltage range	2.1 V
ADC on chip	12 bits
Readout	Serial LVDS
Power consumption	20-40 mW/ch

Details of the SiREAD are provided in Figure 4.3.1 and Table 4.3.1 below. For the programmable logic upgrade the plan is to use an FPGA capable of supporting the high-speed serial interface control and readout of numerous SiREAD. One straw-man design has this single FPGA readout out 16x 64-channel SiREAD, or 4 PMTs worth in the density presented above.

4.3.2 Proposed R&D Activities

FY19

- Integration of the SSP DAQ protocol with the TARGETX/SIREAD front-end chips.
- Characterization of performance and validation of cost for compact and lower power readout variant using the SiREAD ASIC.
- Adaptation of the readout for the use of SiPM arrays.
- Design of a portable DAQ system derived from the CLAS12 RICH readout.

FY20 (tentative)

- Realization and validation of the portable DAQ solution.
- Dedicated tests of SiPM sensors with various level of radiation damage and production technologies, (i..e microcell size, thrences, ...)
- Development of a readout using SiPM arrays with realistic cooling and scalable readout electronics.

4.3.3 Proposed R&D Deliverables

FY19

- Second generation firmware and improved data throughput for front-end to back-end communications
- Integrated system to readout SiPM with temperature control
- Modular and scalable 256-channel building block readout based on the SiREAD ASIC

FY20 (tentative)

- Portable DAQ system for the consortium R&D activities
- Integration of the SSP DAQ protocol with the SIREAD chip

5. Budget

5.1 Budget Request

As our baseline (100% level), we request $461.5k for FY19, but also provide budgets reduced by 20% and 40%, labelled “80%” and “60% in the tables below. We also provide guidance on our plans beyond FY19 in each section above, but do not include summaries in this section for FY20 and beyond. However, please note that in some cases items which would not be funded in the reduced-budget scenarios would be shifted into FY20. Also, please note that the “80%” budget is at the level of the $329k awarded for eRD14

in FY16, while the "60%" level is close to the $244k awarded after the large cuts in FY17, and the $252k received in FY18. The "100%" level is in line with the requests for both FY16 and FY17. All budget items include overhead at the receiving institution. Breakdown of the request by project and institution can be found below for all three funding levels. The consortium funds have been distributed among participating institutions so as to minimize overhead and maximize flexibility. The SOWs will be submitted with wording reflecting the possibility for institutions to fund collaborators at other institutions, for instance to cover travel costs.

5.2 Dual-Radiator RICH (dRICH)

	100%	80%	60%
Postdoc, INFN/JLab, 4 months (Luca Barion)	$12k	$12k	$12k
Postdoc, INFN/JLab, 12 months (Aram Movsisyan)	$35k	$18k	
Prototype components	$5k	$5k	$5k
Total	**$52k**	**$35k**	**$17k**

5.3 Modular Aerogel RICH (mRICH)

	100%	80%	60%
Postdoc, INFN/JLab, 2 months (Luca Barion)	$6k	$6k	$6k
Postdoc GSU (Xu Sun)	$27.3k	$20.5k	$13.7k
Grad student, GSU (William Roth)	$32k	$27.3k	$19.8k
Materials, GSU	$4.5k	$1.5k	$1.5k
Travel and Conference fee, INFN/GSU	$7.5k	$7.5k	$7.5k
Total	**$77.3k**	**$62.8k**	**$48.5k**

5.4 DIRC

	100%	80%	60%
Postdoc, CUA, 50%	$50k		
Graduate student 50%		$30k	
Lens PbF_2	$23k	$23k	$23k
Lens Sapphire	$13k	$13k	$13k
Optical samples for tests of radiation hardness	$5k	$5k	$5k
Radiation Hardness test	$8k	$8k	$8k
Travel, CUA/GSI	$13k	$13k	$13k
Total	**$112k**	**$92k**	**$62k**

5.5 Sensors in High-B Fields

	100%	80%	60%
LHe and materials for high-B run, JLab	$7.6k	$7.6k	$7.6k
Undergraduate student, USC	$10.8k	$5.4k	$5.4k
Travel, USC	$12k	$12k	$12k
High Resolution TDC	$8.8k		
Total	**$39.2k**	**$25k**	**$25k**

5.6 LAPPDs

	100%	80%	60%
Labor	$75k	$60k	$50k
Materials	$15k	$10k	$10k
Travel	$5k	$5k	
Total	**$95k**	**$75k**	**$60k**

5.7 Readout Sensors and Electronics for Detector Prototypes

	100%	80%	60%
Front-end readout electronics, Hawaii	$50k	$30k	$25k
Postdoc, INFN, 6 months (Luca Barion)	$18k	$18k	$18k
Portable DAQ elements	$10k	$5k	
Readout adaptation SiPMs, INFN	$8k	$4k	
Total	**$86k**	**$57k**	**$43k**

5.8 Budget by project

	100%	80%	60%
dRICH	$52k	$35k	$17k
mRICH	$77.3k	$62.8k	$48.5k
DIRC	$112k	$92k	$62k
high-B	$39.2k	$25k	$25k
LAPPD	$95k	$75k	$60k
Electronics	$86k	$57k	$43k
Total	**$461.5k**	**$346.8k**	**$255.5k**

5.9 Budget by institution

	100%	80%	60%
ANL	$95k	$75k	$60k
INFN	$95.5k	$69.5k	$42.5k
CUA (and GSI)	$112k	$92k	$62k
GSU	$69.8k	$55.3k	$41k
U. Hawaii	$50k	$30k	$25k
JLab	$7.6k	$7.6k	$7.6k
USC	$31.6k	$17.4k	$17.4k
Total	**$461.5k**	**$346.8k**	**$255.5k**

Appendices

Appendix A
List of R&D Publications and Presentations

2018 -- Publications

1. X. He, for the EIC PID Consortium (eRD14 Collaboration), *Ring Imaging Cherenkov Detector Technologies for Particle Identification in the Electron-Ion Collider Experiments*, 21st Particle and Nuclei International Conference (PANIC 2017), International Journal of Modern Physics: Conference Series, Vol. 46 (2018) 1960080. DOI: 10.1142/S2010194518600807.
2. J. Xie *et al.*, *Rate capability and magnetic field tolerance measurements of fast timing microchannel plate photodetectors*, NIMA (2018). DOI: 10.1016/j.nima.2017.10.059.
3. G. Kalicy *et al*., *High-performance DIRC detector for the future Electron Ion Collider experiment,* Proceedings of DIRC2017, JINST **13,** C04018 (2018). https://doi.org/10.1088/1748-0221/13/04/C04018
4. Y. Ilieva *et al*., *Particle Identification for a future EIC detector,* Proceedings of DIRC2017, JINST **13,** C03018 (2018). https://doi.org/10.1088/1748-0221/13/03/C03018

2018 -- Presentations

1. X. Sun, for the EIC PID Consortium (eRD14 Collaboration), *Ring Imaging Cherenkov Detector for Particle Identification in the Electron-Ion Collider (EIC) Experiments*, RHIC/AGS Users Meeting, June 12 – 15, 2018.

2017 -- Publications

1. A. Del Dotto, C.-P. Wong *et al*. (EIC PID Consortium), *Design and R&D of RICH detectors for EIC experiments*, NIM A https://doi.org/10.1016/j.nima.2017.03.032
2. J. Wang *et al.*, *Design improvement and bias voltage optimization of glass-body microchannel plate picosecond photodetector*, Nuclear Science IEEE Transactions (in print) 2017.
3. C.P. Wong *et al.*, *Modular focusing ring imaging Cherenkov detector for Electron-Ion Collider experiments*, NIM A 871, 13 (2017).

2017 -- Presentations

1. R. Dzhygadlo for the EIC DIRC Collaboration, *DIRC-based PID for the EIC Central Detector*, oral presentation at the DPG spring meeting, Muenster, March 27 – 31, 2017.
2. X. He for the EIC PID Consortium, *Ring Imaging Cherenkov Detector Technologies for Particle Identification in the Electron-Ion Collider Experiments*, PANIC2017, in Beijing, September 1 – 5, 2017.
3. Y. Ilieva for the EIC PID Consortium, *Particle Identification for a Future EIC Detector*, 2017 International Workshop on Fast Cherenkov Detectors - Photon detection, DIRC design and DAQ, August 7 – 9, 2017, Giessen, Germany.

4. G. Kalicy for the EIC PID Consortium, *The High-Performance DIRC for a Future EIC Detector*, 2017 International Workshop on Fast Cherenkov Detectors - Photon detection, DIRC design and DAQ, August 7 – 9, 2017, Giessen, Germany.
5. J. Xie, *Development of fast-timing microchannel plate photomultiplier*, Fall Meeting of the Division of Nuclear Physics of the American Physical Society (DNP 2017), Pittsburgh, PA, Oct. 2017 (Invited talk)

2016 -- Publications

1. Y. Ilieva *et al.*, *MCP-PMT Studies at the High-B Test Facility at Jefferson Lab*, JINST **11**, 2016; http://dx.doi.org/10.1088/1748-0221/11/03/C03061. Proceedings of the International Workshop on Fast Cherenkov Detectors - Photon detection, DIRC design and DAQ, November 11–13, 2015, Giessen, Germany.
2. G. Kalicy *et al.*, High-performance *DIRC detector for Electron Ion Collider*, submitted to JINST, 2016; Proceedings of the International Workshop on Fast Cherenkov Detectors - Photon detection, DIRC design and DAQ, November 11–13, 2015, Giessen, Germany.
3. J. Xie *et al.*, *Development of a low-cost fast-timing microchannel plate photodetector*, Nucl. Instrum. Meth. A 824 (2016) 159-161.
4. L. Allison: High-performance DIRC detector for use in an Electron-Ion Collider, Proceedings for ICHEP2016 (38th International Conference on High Energy Physics), August 3-10, 2016, Chicago, IL, submitted to Proceedings of Science.

2016 -- Presentations

1. H. Hamilton, *Testing of Advanced Particle Detectors for the Next Generation Particle Collider*, oral presentation at the Abilene Christian University Undergraduate Research Festival, 5 April 2016, Abilene, TX.
2. C. Towell, *Development of an Electron Ion Collider Detector Test Stand*, oral presentation at the Abilene Christian University Undergraduate Research Festival, 5 April 2016, Abilene, TX.
3. A. Del Dotto for the EIC PID consortium, *Design and R&D of RICH detectors for EIC experiments*, poster presented at RICH 2016, 9th International Workshop on Ring Imaging Cherenkov Detectors, Slovenia on September 5-9, 2016.
4. Z.W. Zhao for the EIC PID consortium, EIC RICH R&D, presentation at EIC User Group Meeting, January 2016.
5. L. Allison for the EIC DIRC Collaboration, *Particle ID with DIRC Detectors*, invited talk at ODU Nuclear Group Seminar, March 17, 2016.
6. G. Kalicy for the EIC DIRC Collaboration, *DIRCs*, invited talk at ODU Nuclear Group Seminar, December 4, 2016.
7. G. Kalicy for the EIC DIRC Collaboration, *DIRC@EIC*, presentation at EIC User Group Meeting, January 2016.
8. G. Kalicy: PID systems for the JLab EIC full-acceptance detector, ICHEP2016 38th International Conference on High Energy Physics, August 3–10, 2016, Chicago, IL.
9. J. Xie *et al.*, *Planar microchannel plate photomultiplier with VUV-UV-Vis full range response for fast timing and imaging applications*, accepted for RICH 2016, 9th International Workshop on Ring Imaging Cherenkov Detectors, Slovenia on September 5-9, 2016.

10. C.P. Wong, *Performance Study of a Prototype Modular RICH Detector for EIC Experiments*, oral presentation at 2016 Fall Meeting of the APS Division of Nuclear Physics, October 13–16,2016, Vancouver, Canada.

2015 -- Publications

1. J. Wang *et al.*, *Development and testing of cost-effective, 6cm× 6cm MCP-based photodetectors for fast timing applications*, Nucl. Instrum. Meth. A 804 (2015) 84–93.

2015 -- Presentations

1. H. Hamilton, *Improved Timing Instruments for Particle Identification*, oral presentation at the Abilene Christian University Undergraduate Research Festival, March 31, 2015, Abilene, TX.
2. C. Towell, *Building Detectors to Study a New Phase of Matter*, oral presentation at the Abilene Christian University Undergraduate Research Festival, March 31, 2015, Abilene, TX.
3. E. Bringley *et al.*, *Experimental Setup and Commissioning of a Test Facility for Gain Evaluation of Microchannel-Plate Photomultipliers in High Magnetic Field at Jefferson Lab*, poster presentation at the University of South Carolina Discovery Day, 24 April 2015, Columbia, SC.
4. C. Barber, *Gain Evaluation of Micro-Channel-Plate Photomultipliers in the Upgraded High-B Test Facility at Jefferson Lab*, poster presentation at the Conference Experience for Undergraduates at the 2015 Fall Meeting of the APS Division of Nuclear Physics, October 28–31, 2015, Santa Fe, NM; BAPS.2015.DNP.EA.37.
5. H. Hamilton, *Testing of multigap Resistive Plate Chambers for Electron Ion Collider Detector Development*, poster presentation at the Conference Experience for Undergraduates at the 2015 Fall Meeting of the APS Division of Nuclear Physics, October 28–31, 2015, Santa Fe, NM; BAPS.2015.DNP.EA.9.
6. C. Towell, *Cosmic Test Stand Development for Electron Ion Collider Detector R&D*, poster presentation at the Conference Experience for Undergraduates at the 2015 Fall Meeting of the APS Division of Nuclear Physics, October 28–31, 2015, Santa Fe, NM; BAPS.2015.DNP.EA.20.
7. Y. Ilieva for the EIC DIRC Collaboration, *MCP-PMT Studies at the High-B Test Facility at Jefferson Lab*, invited talk at the International Workshop on Fast Cherenkov Detectors - Photon detection, DIRC design and DAQ, November 11–13, 2015, Giessen, Germany.
8. G. Kalicy for the EIC DIRC Collaboration, *High-performance DIRC detector for Electron Ion Collider*, invited talk at the International Workshop on Fast Cherenkov Detectors - Photon detection, DIRC design and DAQ, November 11–13, 2015, Giessen, Germany.
9. L. Allison for the EIC DIRC Collaboration, *Studies of prototype 3-component lens in CERN test beam and on a test bench at ODU*, invited talk at the International Workshop on Fast Cherenkov Detectors - Photon detection, DIRC design and DAQ, November 11–13, 2015, Giessen, Germany.
10. G. Kalicy for the EIC DIRC Collaboration, *DIRC detectors*, presentation at JLab seminar, Newport News, December 2015.
11. G. Kalicy for the EIC DIRC Collaboration, *Photosensors tests at high B facility in JLab*, presentation at meeting with Photonis in Lancaster, PA,October 2015.
12. G. Kalicy for the EIC DIRC Collaboration, *Photosensors tests at high B facility in JLab*, presentation on meeting with Hamamatsu at JLab, September 2015.

13. G. Kalicy for the EIC DIRC Collaboration, *Developing DIRC Technology*, presentation at ODU Colloquium, Norfolk VA, April 2015.
14. R. Dzhygadlo for the EIC DIRC Collaboration, *DIRC-based PID for the EIC Central Detector*, oral presentation at the DPG spring meeting, Heidelberg, March 23–27, 2015.
15. C.P. Wong, *Simulation Study of RICH Detector for Particle Identification in Forward Region at Electron-Ion Collider*, oral presentation at APS April Meeting 2015, April 11–14, 2015, Baltimore, MD.

Prior 2015 -- Presentations

1. C. Nickle, *Experimental Setup for Magnetic-Field Tests of Small-Size Light Sensors at Jefferson Lab*, poster presentation at the Conference Experience for Undergraduates at the 2013 Fall Meeting of the APS Division of Nuclear Physics, October 23–26, 2013, Newport News, VA; BAPS.2013.DNP.EA.121.
2. E. Bringley *et al.*, *Experimental Setup and Commissioning of a Test Facility for Gain Evaluation of Microchannel-Plate Photomultipliers in High Magnetic Field at Jefferson Lab*, poster presentation at the Conference Experience for Undergraduates at the 4th Joint Meeting of the APS Division of Nuclear Physics and the Physical Society of Japan, October 7–11, 2014, Waikoloa, Hawaii; BAPS.2014.HAW.GB.140.
3. H. Hamilton, *Time of Flight Detector Development for Future Heavy Ion Experiments*, poster presentation at the Conference Experience for Undergraduates at the 4th Joint Meeting of the APS Division of Nuclear Physics and the Physical Society of Japan, October 7–11, 2014, Waikoloa, Hawaii; BAPS.2014.HAW.GB.149.
4. C. Towell, *Developing a High Precision Cosmic Test Stand for PHENIX Research and Development*, poster presentation at the Conference Experience for Undergraduates at the 4th Joint Meeting of the APS Division of Nuclear Physics and the Physical Society of Japan, October 7–11, 2014, Waikoloa, Hawaii; BAPS.2014.HAW.GB.147.